MICHIGAN STATE UNIVERSITY LIBRARIES
3 1293 00792 7365

This is to certify that the

thesis entitled

Design and Construction of a Multichannel

detector for Flow Injection Analysis
presented by

Edwin Josue Castellanos

has been accepted towards fulfillment
of the requirements for

~~Master~~ degree in Chemistry

Major professor

Date August 7, 1992

O-7639 *MSU is an Affirmative Action/Equal Opportunity Institution*

LIBRARY
Michigan State
University

PLACE IN RETURN BOX to remove this checkout from your record.
TO AVOID FINES return on or before date due.

DATE DUE	DATE DUE	DATE DUE

MSU Is An Affirmative Action/Equal Opportunity Institution
c:\circ\datedue.pm3-p.

DES

DESIGN AND CONSTRUCTION OF A MULTICHANNEL DETECTOR FOR FLOW INJECTION ANALYSIS

By

Edwin Josué Castellanos

A THESIS

Submitted to
Michigan State University
in partial fulfillment of the requirements
for the degree of

MASTER OF SCIENCE

Department of Chemistry

1992

ABSTRACT

DESIGN AND CONSTRUCTION OF A MULTICHANNEL DETECTOR FOR FLOW INJECTION ANALYSIS

By

Edwin Josué Castellanos

A novel flow-through photometer suited for Flow Injection Analysis was constructed and tested. The new detector features a multichannel parallel design especially suited for multideterminations in flowing systems. The simple photometer uses an LED as light source to avoid the need for a wavelength selection device. A reference photodiode in a feedback loop controls the forward current for the LED, assuring a constant level of light. The observation cell in every channel is constructed of Delrin and Kel-F and every component is removable.

The figures of merit for the new photometer are determined by the type of LED used in a given determination. In the present thesis, the detector was used in the enzymatic determination of sugars in food samples using the leucomalachite green-H_2O_2 detection reaction. The calibration curves were linear up to absorbances of 0.9. The deviation from linearity was mainly caused by a polychromatic light effect. The sensitivity of the detector to variations in the flowing liquid limited the precision of the measurements. Still, the results were satisfactory when the new detector was used in the glucose determination in apple juice.

To my wife Kelly Anne
and my family in Guatemala,
especially my mother.

ACKNOWLEDGMENTS

Special thanks to Dr. Crouch for his guidance thoroughout this research and for his promptness in correcting the manuscript despite a busy summer of '92.

People who were of great help in completing parts of this project include: Marty Rabb, electronic designer, for his advice on improving the circuits of the detector; Kris Kurtz for providing the reactors (both plain and enzymatic) for the experiments; Pavlos Aspris for the hints on the leucomalachite green reaction; Steve Medlin for his help when things were not so smooth with computers; and Brett Quencer for recording some of the LED spectra with a diode array detector.

The support of my wife, my parents-in-law, and my family was key in succesfully completing this work.

List o
List o
INTR
CHA
CHA
CHA

TABLE OF CONTENTS

	PAGE
List of Tables	vii
List of Figures	viii
INTRODUCTION	1
CHAPTER I: Photometric Detectors for Flow Injection Analysis	3
A. Flow Injection Analysis and its use with other Techniques	3
B. LED-based Flow-through Photometric Detectors	5
C. Multidetermination and Multidetection	7
CHAPTER II: Overview of the Detector	12
A. The Sugars Analyzer	12
B. The Multichannel Detector	16
CHAPTER III: Design and Construction of the Flow-through Photometer	23
A. The Photometric Cell	23
1. Choice of Materials	23
2. Design and Construction	25
3. Choice of Components	30

PAGE

B. The System Electronics 36

1. Light Regulation Electronics 36

2. Signal Processing Electronics 39

CHAPTER IV: Operation and Characterization of the Detector 42

A. Operation Procedures 42

1. Initial Operation 42

2. Adjusting the Light Level 43

B. Characteristics of the Detector 45

1. Sensitivity to Flow Variations 47

2. Baseline Noise and Drift 52

3. Peak Broadening 56

4. Dynamic Range 58

5. Precision of Measurements 80

6. Detection Limit 88

C. Practical Application 88

CHAPTER V: Conclusions and Recommendations 92

References 96

Table
Table
Table
Table

LIST OF TABLES

		PAGE
Table 2-1	Description of Features Included in the Multichannel Detector to Fulfill Specific Requirements of the Sugar Analyzer	20
Table 4-1	Results of the Experiment of Repeatability of Measurements with the LED-Based and Patton's Photometers	85
Table 4-2	Relative Standard Deviations for the Triplicate Readings of the Solutions in two Calibration Curves	87
Table 5-1	Experimental Results for a Single Photometer of the Multichannel Detector	95

Figur
Figur
Figur
Figur
Figur
Figur
Figu
Figu
Figu
Figu
Figur
Figur

LIST OF FIGURES

		PAGE
Figure 1-1	Possibilities for Multidetection and Multideterminations using Flow Injection Analysis.	9
Figure 1-2	Schematic diagrams of FIA manifolds for obtaining sequential multidetection.	10
Figure 2-1	Parallel multichannel flow injection analyzer for enzymatic determination of sugars.	14
Figure 2-2	Enzymatic methods for the determination of the six sugars.	15
Figure 2-3	Schematic diagram of the six channel detector. Channel 2 is omitted for clarity.	18
Figure 2-4	Schematic diagram showing the different components of the photometer in every channel of the detector.	19
Figure 3-1	Construction of the photometric cell used in every channel of the detector (drawn to scale).	27
Figure 3-2	Main body of the photometric cell made of Delrin. All measurements in inches (drawn to scale).	28
Figure 3-3	Other components of the photometric cell: a) photodiode socket (Delrin); b) LED socket (Delrin); c) observation cell (Kel-F). All measurements in inches (drawn to scale).	29
Figure 3-4	Absorption spectrum of malachite green, the substance detected in the enzymatic determination of sugars.	31
Figure 3-5	Emission spectrum of a ultrabright type LED from Radio Shack.	33
Figure 3-6	Emission spectra of two available LED's for the detection of the malachite green.	34

		PAGE
Figure 3-7	Light regulating circuit. The current produced by the reference photodiode controls and regulates the intensity of the LED.	37
Figure 3-8	Signal processing circuit.	40
Figure 4-1	Schematic diagram of the FIA manifold used in the experiments to characterize the multichannel detector.	46
Figure 4-2	Injection of a 0.04 mM solution of hydrogen peroxide. The noise in the signal came from the pump oscillation. The flow rate was 1.3 ml/min.	48
Figure 4-3	Stabilization device used in the carrier channel after the pump to reduce the effect of its oscillations.	50
Figure 4-4	Injection of a 0.04 mM solution of hydrogen peroxide using two stabilization devices: one in the carrier channel and one in the sample channel. The small peak at 8 seconds was caused by the injection process.	51
Figure 4-5	Injection of a 0.04 mM solution of hydrogen peroxide using a larger observation cell. The noise in the signal came from the pump oscillation. The flow rate was 1.3 ml/min.	53
Figure 4-6	Injection of a 0.04 mM solution of hydrogen peroxide using a larger observation cell and one stabilization device in the carrier channel.	54
Figure 4-7	Dispersion patterns for both detectors at low and high sample concentrations.	57
Figure 4-8	Calibration curve using LMG-hydrogen peroxide with stock solution of LMG 1.5 mM.	60
Figure 4-9	Calibration curve using LMG-hydrogen peroxide with stock solution of LMG 3.0 mM.	62
Figure 4-10	Calibration curve using LMG-hydrogen peroxide with stock solution of LMG 1.5 mM using two sizes of observation cells.	64
Figure 4-11	Calibration curve using LMG-hydrogen peroxide with stock solution of LMG 9.0 mM. The LED detector was used with the three available LED's.	66

		PAGE
Figure 4-12	Calibration curve using LMG-hydrogen peroxide with stock solution of LMG 10.0 mM. The LED at 610 nm was used in Patton's detector with and without a filter.	69
Figure 4-13	Calibration curve using LMG-hydrogen peroxide with stock solution of LMG 10.0 mM. The LED detector was used with LED forward currents of 10 and 30 mA.	71
Figure 4-14	Emission spectra for the LED at 610 with low and high forward currents.	73
Figure 4-15	Absorption spectrum of methylene blue in water.	74
Figure 4-16	Calibration curve using methylene blue at 610 and 660 nm.	76
Figure 4-17	FIA peaks observed with the calibration curve using prepared malachite green.	78
Figure 4-18	Calibration curve using malachite green previously prepared.	79
Figure 4-19	9 injections of a 0.04 mM solution of H_2O_2 using the LED-based detector. The RSD of the measured absorbance is 2.63%.	81
Figure 4-20	9 injections of a 0.04 mM solution of H_2O_2 using Patton's detector. The RSD of the measured absorbance is 1.62%.	82
Figure 4-21	8 injections of a 0.08 mM solution of H_2O_2 using the LED-based detector. The RSD of the measured absorbance is 2.25%.	83
Figure 4-22	8 injections of a 0.08 mM solution of H_2O_2 using Patton's detector. The RSD of the measured absorbance is 1.95%.	84
Figure 4-23	Calibration curve for the glucose content determination in apple juice.	90

INTRODUCTION

Analytical chemists are always in the search of simple instruments that can replace tedious manual methods or long instrumental determinations and perform in a faster and more reliable way. Flow Injection Analysis (FIA) has proven to be very effective in this sense, making the handling of liquid samples an easier task.

The determination of sugars in food samples is an example of an analytical procedure that is not always suited to the changes and needs of modern industry. The official method of analysis dictated by the Association of Analytical Chemists is a non-selective volumetric method that can only determine the total amount of sugars present [1] but not the individual concentrations of specific sugars. To accomplish the latter, the use of High Performance Liquid Chromatography (HPLC) is recommended, a procedure which can be very elaborate and time consuming.

The work presented in this thesis is part of a larger research project in Dr. Crouch's group which aims at the construction of a novel analyzer for sugars in food samples based on immobilized enzymes and FIA principles. The system will provide a fast and simple way of determining up to six nutritionally important sugars in food samples with complex matrices without prior separations. Work on the project has been going on for several years already, with various researchers focusing on different aspects, such as immobilization processes, sample preparation, and construction of the FIA manifold [2-6].

My part in the project was to construct a simple and inexpensive detector with a parallel design; that is, a detector able to monitor six different flowing streams simultaneously. The determinations are based on photometric measurements using LED's as light sources.

A goal of the research was to build a detector suited to the needs of the sugars analyzer but applicable also to a FIA system in general.

The sequence of the chapters follows the way the project was completed. The first chapter reviews the work done in the area by other researchers, whose ideas gave origin to my project. In the second chapter, the detector is presented as part of the complete sugars analyzer to show how the characteristics of the final instrument influence the requirements for the detector. Then, in the third chapter, a more detailed description of the detector is included beginning with the design process of the flow-cell. This chapter ends with a discussion of the detector electronics. Chapter IV presents the experiments performed in order to fully characterize the new detector and to compare it to the one currently in use. The thesis ends in Chapter V with conclusions and recommendations concerning how to attain an optimum performance from the detector.

CHAPTER I

PHOTOMETRIC DETECTORS FOR FLOW INJECTION ANALYSIS

One of the most attractive characteristics about FIA is the simplicity of the instrumentation needed. Much effort has gone into keeping the system simple, including the detector. A simple photometer with a LED as the light source has provided excellent results for this purpose. This chapter reviews the work done to construct such flow-through photometers, work that was used to develop the ideas for the six-channel detector described in this thesis. A brief presentation of FIA and its many applications with different analytical techniques precedes the review as a means of introduction. The chapter concludes with a discussion of the different possibilities in FIA for a multidetermination of analytes in a sample.

A. FLOW INJECTION ANALYSIS AND ITS USE WITH OTHER TECHNIQUES

Flow Injection Analysis (FIA) has developed throughout the past decade as an important method of analysis due to its versatility and simplicity [7,8]. The basic components of a FIA system (pump, injection valve, reaction coil, and detector) can be arranged in many different ways to adapt to applications in such varied fields as agriculture, biochemistry, food science, and clinical chemistry, to name but a few.

Many review articles in the different areas of application are available in the literature as well as three monographs [7-14]. The reader is referred to those sources for a comprehensive description of the available methodology.

As noted by Poppe [15], the definition of a detection system in FIA can be ambiguous. In many cases the FIA system is much simpler than the detection system, so that it is no longer valid to talk of a detector for FIA; rather, it is more accurate to say that the FIA apparatus serves as a sample introduction system for the more complex instrument. It also happens, with techniques such as HPLC, that the detection device is the whole flow injection system itself, with the sample being delivered by the chromatographic separation unit instead of being injected [16]. In any case, FIA systems have made easier the task of sample handling before a final instrumental measurement.

FIA has been used in conjunction with a variety of detectors and analytical techniques. It would be impossible in the short space of this work to review even briefly the different methods that may be used in FIA. Just to give an idea, the monograph by Ruzicka and Hansen [7] lists seventeen spectrometric methods, eight electrochemical methods, nine separation methods, eleven gradient techniques, kinetic methods (enzymatic and non-enzymatic), plus a variety of less common techniques such as enthalpimetry and viscosimetry.

Spectrophotometry is by far the most widely used detection technique, employed in more than 40% of the published papers [7]. A reason for this is the fact that spectrophotometry is the most common analytical technique, so there are methods available to determine almost any type of analyte. Also, it is very easy to adapt a spectrophotometer to

a FIA system provided that its optical components produce a light beam small enough in diameter to be sent through flow cells of small apertures. A flow cell of the Hellma type is commonly used, but the so-called Z cell is also very well-suited [7].

Two optical techniques that are gaining popularity in the FIA field are atomic absorption (AAS) and inductively coupled plasma spectrometry (ICP). FIA has proven to be an excellent injection system for these instruments, increasing their sensitivity over 100 times [17,18].

Apart from the optical techniques, electrochemical methods have also been coupled with success to FIA systems, and research is directed now to the miniaturization of electro-sensors and the use of ion-selective field effect transistors (ISFET's) [19].

B. LED-BASED FLOW-THROUGH PHOTOMETRIC DETECTORS

In a conventional design of a FIA system using spectrophotometric detection, the flowing stream with the sample has to be taken back and forth from the FIA manifold into the spectrophotometer adapted with a flow-through cell. Conceptually, it is better to introduce the detector into the manifold system rather than to pump the carrier stream into the detector, thus avoiding extra tubing and higher dispersion. If the use of a spectrophotometer is necessary, this can be accomplished by using fiber optics to transport the light to the manifold [20].

In many cases, though, a full spectrophotometer is not needed. If the FIA system is to be used only on a specific chemical determination, the wavelength selection capability of a spectrophotometer becomes superfluous, and the measurements can be made with a simple photometer. If a light source with a narrow emission band is used, a

filter to isolate a given wavelength is not needed, which simplifies the photometer even further.

A light emitting diode (LED) emits light with a bandwidth ranging from 20 to 50 nm which is monochromatic enough for the purposes of most FIA determinations. A photometric measurement in the visible region can thus be carried out using the LED as the light source and a photodiode or phototransistor as the light detector.

The replacement of the tungsten lamp by a LED for photometric determinations in the visible region is nowadays more feasible with the commercial availability of ultra-bright LED's. This special type of LED can reach luminous intensities as high as 5 candelas (about 1000 times brighter than normal LED's). The brightest LED's available emit at 660 nm, the natural wavelength of emission for the Gallium Phosphide pn junction. Doped Gallium Phosphide LED's are available at lower wavelengths and lower brightnesses, typically of 0.3 candelas [21].

An advantage of LED's over conventional tungsten lamps is their low power consumption. LED's typically dissipate 75 mW, compared to 3 to 5 W for miniature tungsten lamps. Despite using considerably less power, LED's can still attain high luminous intensities due to narrow bands of emission and high luminous efficacies.

The first applications of LED-based photometers for analytical purposes were to static systems [22,23]. Betteridge et al. [24] applied the idea to design a flow-through LED-based photometric detector for FIA. The detector was extremely simple and inexpensive, having the LED and phototransistor glued in a block of plastic with holes drilled in it to form the flow-cell. Despite its simplicity, the detector proved to have an adequate level of sensitivity and detection limit.

Sly and co-workers [25], from the Betteridge laboratories, improved the original detector by designing a more flexible circuit that allowed different gains and LED currents, and by placing the LED and phototransistor perpendicular to the flowing stream and outside the carrying tube. The detector showed better resolution, but higher detection limits. The sensitivity was maintained by the improved amplification circuit.

A variation of this principle was implemented by Hooley and Dessy [26] in a system with a multi-LED detector for kinetic studies in flow systems. They combined the ideas of Sly [24] and Anfält [23] et al. to construct a detector with the light path perpendicular to the flowing stream, and with improved circuitry: the light source was modulated to reduce the effects of ambient light, and a reference photodiode was added in a feedback loop to monitor the light from the LED and keep its intensity constant. A total of eight detection heads were used to monitor the reaction mixture at different positions along the manifold.

Still another modification to the original detector of Betteridge et al. was made by Trojanowicz et al. [27]. The detector built by this group had removable holders for the LED and the photodiode, making their replacement an easy task. This is an important feature since different LED's have to be used for different determinations.

C. MULTIDETERMINATION AND MULTIDETECTION

The flexibility of a FIA system offers the choice of several solutions for a given problem. A good example is found in multideterminations (the determination of two or more analytes in a sample) such as determining six sugars in food samples. The first decision is whether the analysis will be sequential, determining *n* analytes from *n* sequential

injections of the same sample, or simultaneous, doing the entire analysis from a single injection. The simultaneous choice calls for multidetection.

Multidetection, as defined by Luque de Castro and Valcárcel [28], refers to obtaining two or more signals from a single injected sample. To accomplish this, the options are several [29,30]; a summary of them is presented in Figure 1-1. From the study of Figure 1-1 and from the preceding discussion, it can be deduced that a multidetermination can be achieved by multidetection, but multidetection does not necessarily produce a multidetermination. An example of the second situation is found in the use of FIA for kinetic studies, where several signals at different times are obtained from the same chemical system.

Figure 1-2 shows examples of FIA manifolds to obtain sequential multidetection. The arrangement of several detectors in series (Figure 1-2 c) is most adequate for kinetic measurements. For other types of measurements, the choice of a single detector (Figure 1-2 a,b) or several detectors in parallel (Figure 1-2 d,e) depends on the nature of the chemical composition of the individual channels. If the systems are compatible, they can be mixed at the end, and only one detector is needed for the determination; otherwise, several detectors in parallel are required. For our system, the option of six detectors in parallel is preferred not for the incompatibility of chemical systems (all the channels will carry the same reagents with slightly different pH's), but rather for time reasons: waiting for six peaks to elute through one detector would substantially increase the time of analysis.

A single injection (Figure 1-2 d) will also help to keep the time of analysis short. Low reproducibility in equally splitting a small sample

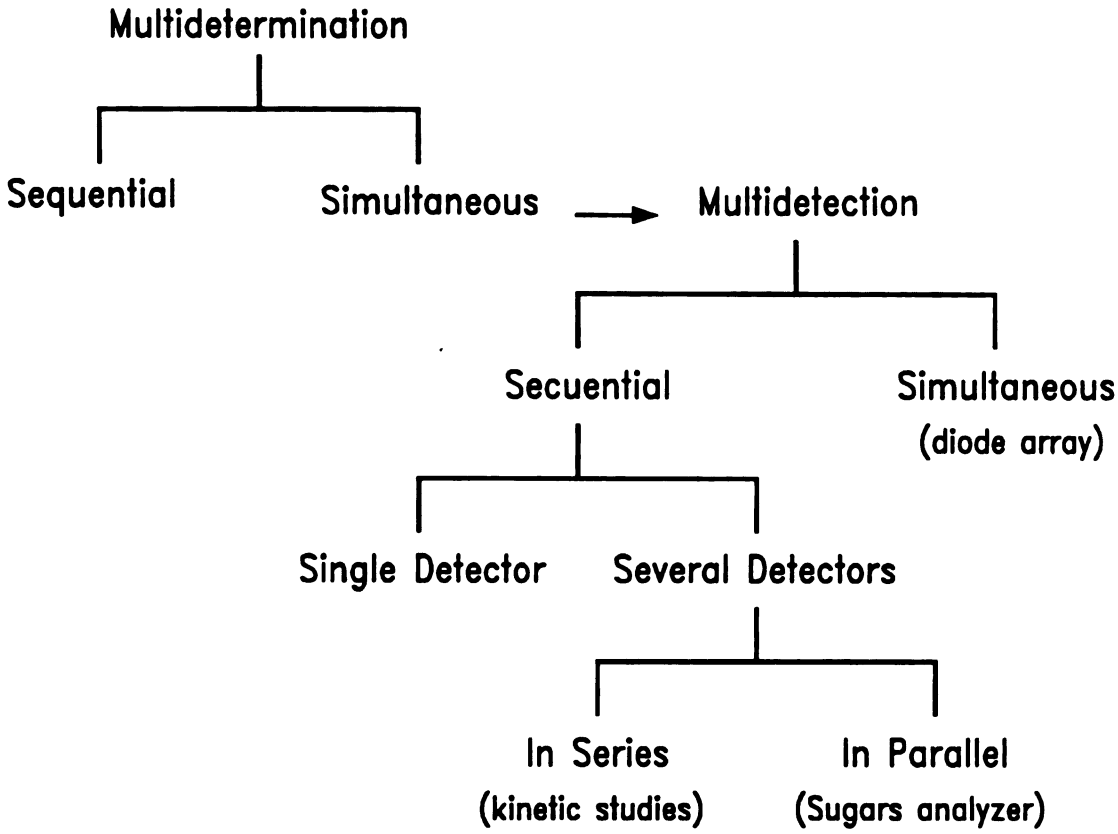

Figure 1-1: Possibilities for Multidetection and Multidetermination using Flow Injection Analisis.

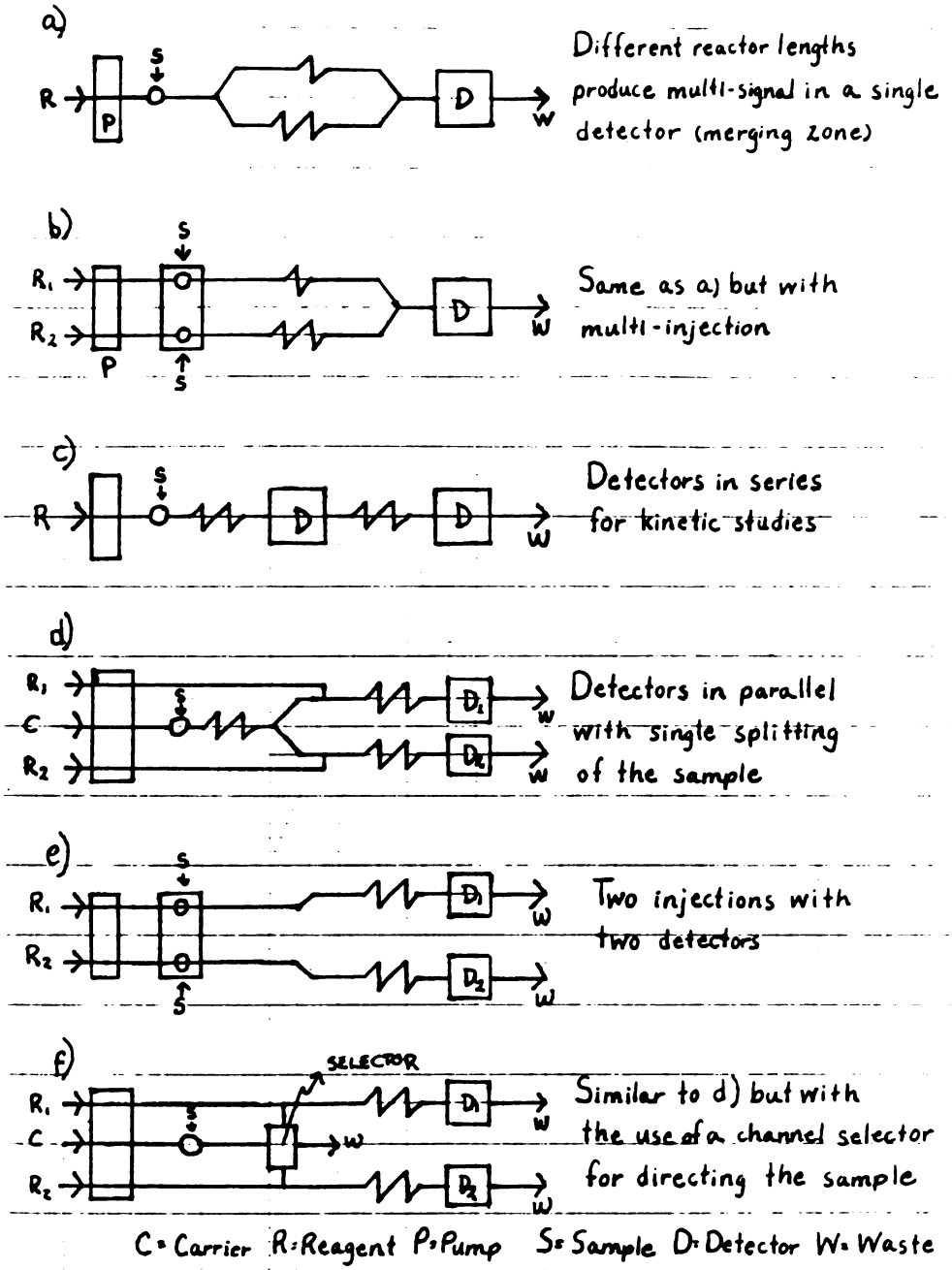

Figure 1-2: Schematic diagrams of FIA manifolds for obtaining sequential multidetection.

into six portions could be problematic; a simultaneous multiple injection may avoid this situation (Figure 1-2 e, f).

The sugars analyzer under construction in our laboratories, will then, make a simultaneous multidetermination of sugars in food samples from a single injection, or at least from a simultaneous multi-injection, and the detection will be sequential with six detectors in parallel.

CHAPTER II

OVERVIEW OF THE DETECTOR

In the first part of this chapter, a brief description of the sugars analyzer under construction in our laboratories gives background information for introducing the multichannel detector. The ideas from other researchers for LED-based detectors, presented in Chapter I, were adapted to the specific detection requirements of the multichannel sugars analyzer. This chapter presents a study of those requirements and gives a general overview of the features of the detector. A more detailed description of its design and construction is given in Chapter III.

A. THE SUGARS ANALYZER

Work on different aspects of continuous flow analysis has been going on for over a decade in our group, so it is difficult to define exactly when the first research concerning the sugars analyzer was done.

The idea of determining six sugars in food samples simultaneously was first suggested by Stults [4] who used a FIA system designed by Patton [3]. Previously, Thompson [2] had determined glucose using FIA. These are probably the first projects closely related to the FIA sugars analyzer as it is being currently used.

With the final version of the FIA sugars analyzer, the determination of up to six sugars in food samples will be simpler and faster (as

compared to traditional methods such as HPLC) for two main reasons: first, the highly parallel design of the system, and second, the elimination of any prior separations, since the selectivity for each sugar is achieved by the use of specific enzymes. An ultimate goal is to produce a miniature analyzer that operates on battery power so that it can be taken into the field for speedy determination of sugars in, for example, fruit juices, in order to determine the optimum harvest time.

Stults [4,31] worked on the optimization of a single channel glucose analyzer using immobilized glucose oxidase. It was suggested later that this concept could be extended to make a parallel multichannel sugars analyzer, as shown in Figure 2-1. Within this scheme, each sugar is converted to its oxidized form by the action of the enzyme reactor containing the corresponding oxidase with the release of hydrogen peroxide. Figure 2-2 shows the enzymatic reactions used to determine the six sugars. Kurtz worked on the immobilization procedures for the enzymes involved [5].

The H_2O_2 released by the oxidation reaction of sugars can be detected by reacting it with a dye in the presence of horseradish peroxidase. The change in color in the oxidized dye is detected colorimetrically. Therefore, the simultaneous determination of the six sugars can be accomplished by detecting the appearance of a single colored substance: an oxidized dye.

There are several reactions involving the oxidation of a dye by hydrogen peroxide. The Trinder reaction [32],

$$H_2O_2 + AAP + DCPS \xrightarrow{\text{peroxidase}} \text{red dye} + H_2SO_4$$

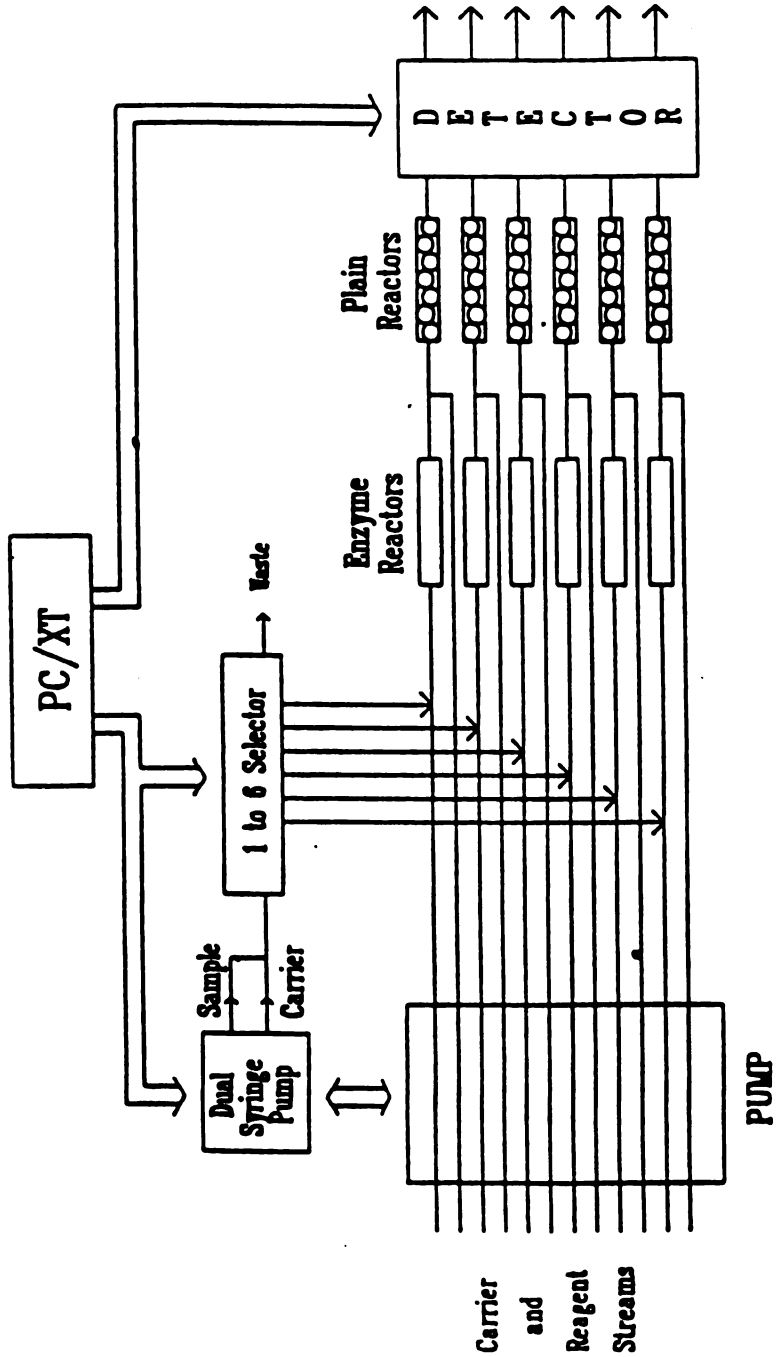

Figure 2-1 Parallel multichannel flow injection analyzer for enzymatic determination of sugars.

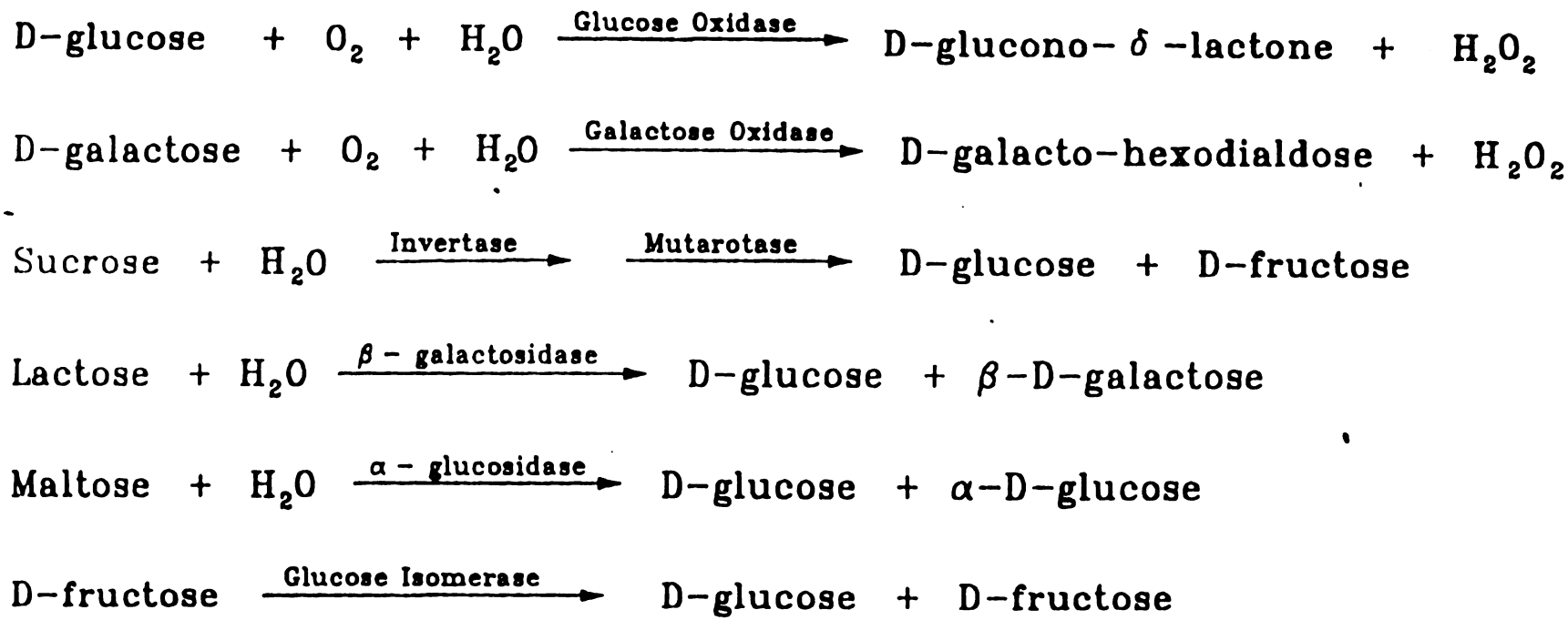

Figure 2-2 Enzymatic methods for the determination of the six sugars.

where AAP = 4-aminoantipyrine and DCPS = 3,5-dichloro-2-hydroxyphenyl sulfonic acid, was the first option investigated. Later, the oxidation of the leucomalachite green (LMG) reaction to form the highly colored malachite green (MG):

$$H_2O_2 + LMG \xrightarrow{peroxidase} MG + H_2O$$

was found to give higher sensitivity and lower detection limits. The reaction was optimized by Aspris [6] who investigated the application of the analyzer to real samples.

All previous research in our laboratories has been done with a FIA system designed by Patton [3]. This system uses a simple dual-beam photometer [33] to monitor the formation of the colored dye. The photometer uses a miniature tungsten-halogen lamp as light source and a bifurcated fiber optic that serves two functions: to split the beam to produce a reference; and to transport the main beam to the observation cell. This cell is a commercial flowcell (PN 178-13724-02, Technicon Instruments; Tarrytown, NY) with sapphire windows, 1.0 cm pathlength, and 0.05 cm internal diameter. The wavelength of interest is isolated by interference filters that can be exchanged to suit the particular application. This type of detector has been applied only as a single-channel analyzer.

B. THE MULTICHANNEL DETECTOR

From the above discussion of the sugars analyzer, it can be seen that the instrument is a typical example of the case discussed in Chapter I in which a full spectrophotometer serving as detector is unnecessary. No wavelength selection capability is needed since the species to be determined is always the same.

The concept of a LED-based photometer was applied to construct the six-channel detector schematically shown in Figure 2-3. Basically, the instrument consists of six independent, LED-based, flow-through photometers such as the one in Figure 2-4 placed in parallel. Detailed drawings and specifications describing materials and components, construction, and dimensions are found in chapters III and IV. The remainder of this chapter is dedicated to an overall description of the various features of the detector.

Table 2-1 summarizes the general requirements for the detector, as well as the features included in the instrument that satisfy these requirements.

Each one of the individual photometers composing the multichannel detector (Figure 2-3) is seen to have three main parts: the measuring cell, the light regulating electronics, and the signal processing electronics.

The measuring cell (Figure 2-4) is made of black plastic and houses the observation cell which consists of a cylinder made of Kel-F with holes for the flowing stream drilled in it. The side of the observation cell facing the LED has a lens to focus the light, and the other side features a glass window. This cell is connected to the rest of the FIA system by stainless steel tubes. The measuring cell has two removable holders for the LED and two photodiodes, one of them looking at the tip of the LED and the other one at the other side of the observation cell.

The light level from the LED is kept constant by means of the photodiode next to it. The photocurrent produced by this reference photodiode is converted to a voltage and then compared to a reference

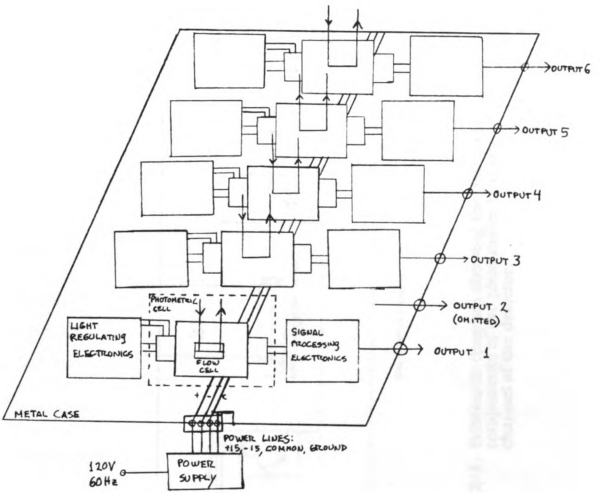

Figure 2-3: Schematic diagram of the six channel detector. Channel 2 is omitted for clarity.

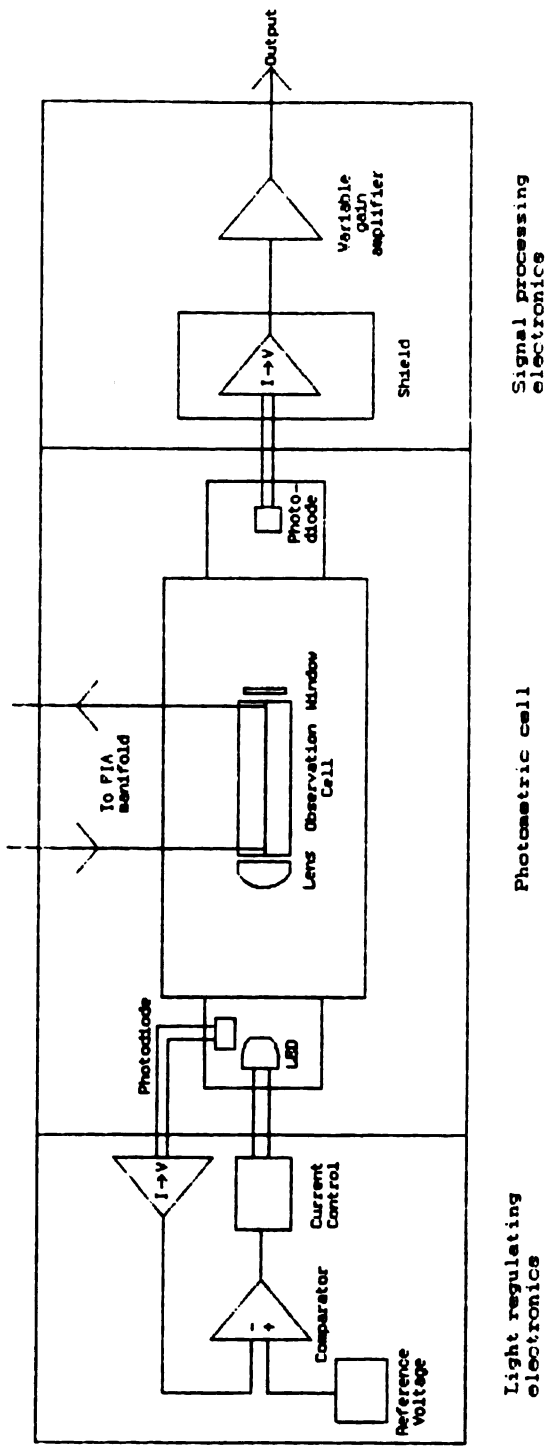

Figure 2-4: Schematic diagram showing the different components of the photometer in every channel of the detector.

Table 2-1:

Description of Features Included in the Multichannel Detector to Fulfill Specific Requirements for the Sugar Analyzer

Requirement of system:	Feature of detector:
1- Fixed Wavelength	Easily done with LED as light source
2- Simple	Use of LED eliminates need for monochromator and/or filters
3- Inexpensive	Can be constructed in-house
4- Low energy requirement	LED's suitable for battery operation
5- Portable	Weight less than 5 lb. (without power supply); small size
6- Replaceable parts	All active components in removable holders
7- Rapid Response	Six signals can be monitored simultaneously. User can choose number of channels to use
8- Adjustable gain	Gain adjustable from 1 to 60
9- Broad working range, adequate sensitivity and detection limit.	Parameters adjusted by selecting different LED's or by changing driving currents

voltage. The output of this comparator controls the amount of current supplied to the LED, and will vary it to counteract any light variations.

The current from the photodiode across the observation cell, which is linearly related to the transmittance of the liquid in the cell, is converted to voltage and then amplified with a variable gain amplifier. This gives the final output signal of the detector.

As previously mentioned, using LED's as light sources is an excellent alternative when no wavelength selection capability is needed. In the multichannel detector, the LED is easily removed, thus providing additional flexibility in choosing the wavelength of analysis. High brightness LED's with peak emissions at various wavelengths in the visible spectrum are available from different manufacturers for the determination of analytes absorbing visible light.

The use of LED's greatly simplifies the photometer and eliminates wavelength isolation components, which in turn reduces the price of the detector. Likewise, a reduction in cost is achieved by replacing the commercial miniature flow-cell, with prices as high as $200, with a flow-cell constructed from a piece of plastic material with the necessary holes drilled in it. Keeping the costs of individual detectors low is important when six of them are going to be used.

Apart from simplifying the instrument, LED's require considerably less power than tungsten lamps. This is an important factor to consider if the instrument is operated on batteries. Battery operation capability is a desirable feature in an instrument that might be taken to the field. Light weight (less than 5 pounds without power supply), and small dimensions (the six detectors are enclosed in a 12"x15" case) also contribute to the portability of the detector.

The design and construction of the instrument provide easy revision and maintenance of the different parts. All the active electronic components are easily removable, as are the parts in the plastic observation cell.

With respect to output characteristics, the parallel design for the six channels will keep the time of analysis per sample similar to that for the determination of a single sugar. The output level is adjustable by means of a variable gain amplifier to compensate for solutions of different absorbances.

The three important characteristics for a detector —linear range, sensitivity, and detection limit— may be adjusted by using different LED's and by varying the current driving them. Using the brightest LED available, with peak emission at 660 nm and narrower bandpass, will give the broadest dynamic ranges, but for the detection of malachite green, with a peak absorption at 618 nm, the sensitivity will be low and the detection limit subsequently high. The use of a LED with peak emission closer to 618 nm with lower brightness and broad bandpass will increase the sensitivity and lower the detection limit at the expense of reducing the dynamic range. The brightness of the LED can be increased by increasing the current driving it, but not without two drawbacks: increased emission bandwidth and reduced lifetime.

CHAPTER III

DESIGN AND CONSTRUCTION OF THE FLOW-THROUGH PHOTOMETER

We saw in the previous chapter that the multichannel detector is simply a set of six independent photometers operated simultaneously. This chapter includes a detailed description of the design and construction of one of these photometers. This work was completed in two phases: construction of the photometric cell and construction of the electronics. This chapter is divided accordingly in two main sections.

A. THE PHOTOMETRIC CELL

The construction of the body of the colorimeter took most of the time of the project primarily because of difficulties in machining the different pieces. Two designs were discarded before any tests were done on them because of problems in construction. The observation cell presented a special problem because of its small dimensions.

1. Choice of Materials

Factors taken into consideration in choosing the materials included availability, mechanical and optical characteristics, and resistance to chemical attack. Plastic materials have been the choice in

the construction of previous LED-based photometric flow-cells due to their chemical resistance and light weight.

Trojanowicz et al. [27] used Teflon in their cell. This plastic is well-suited for its opacity and high resistance to chemical attack, but it is difficult to machine, especially when considering the dimensions needed to construct a miniature flow-cell.

Plexiglass was also considered since it has been used in the construction of components for FIA manifolds. This plastic shows excellent mechanical and chemical properties but its transparency would present problems concerning stray light.

The material chosen was black Delrin, a plastic from DuPont with good mechanical properties and low cost. Delrin is readily attacked by solutions of extreme pH (acid or base) [34], so it can only be used in the parts of the colorimeter that will not be in direct contact with any solution. Although the determination of sugars using the enzymatic method discussed in the preceding chapter only involves solutions of moderate pH, and therefore using Delrin in the composition of the cell would pose no problem, using this material would limit the applicability of the detector to other systems. Another problem arises regarding the cleaning of the FIA system, which is usually done after a long period of use by flushing with a 10% solution of nitric acid.

As will be seen later in this chapter, the only part of the colorimeter in direct contact with the flowing solution is the observation flow-cell. This component was made of Kel-F, a white plastic from 3M with superior mechanical properties and great resistance to attack from highly corrosive chemicals [35]. The material was found to be somewhat transparent to light so the sides of the flow-cell had to be painted black.

2. Design and Construction

The main idea in the design of the body of the photometer is to have all the components be replaceable. Although this makes the assembly process slightly more complicated, the machining of the individual pieces is greatly simplified. This proved to be very important in the construction in one of the earlier designs. That design did not feature the flow-cell as a separate part: the holes necessary to make the cell were drilled directly into the main block of the detector. This presented two problems. The walls of the flow-cell had to be of the same material as the entire colorimeter body, in this case Delrin. This would have limited the use of the detector to systems with no extreme pH as discussed earlier. Secondly, it was extremely difficult to drill the miniature holes accurately (1/40" i.d.) to make the flow cell, and if an error were made the entire block had to be discarded.

A second factor that affected the final design of the detector was the implementation of a reference channel to regulate the amount of light from the LED. An earlier design attempted to use a rudimentary beam splitter like the one reported by Hooley and Dessy [26]. It consists of a glass rod with polished sides, with one of the ends cut at a 45° angle. This "beam splitter" is actually a reflecting device that produces a 90° deviation, and the splitting of the beam comes from imperfections at the surface that scatter some of the light. Most of the light is then perpendicularly directed from the LED. In the design by Hooley and Dessy [26] the main photodetector was located at a 90° angle from the LED, thus receiving most of the light. A similar configuration was difficult to implement in the new LED detector, so this beam splitter design could not be used.

The final design of the colorimeter is illustrated in Figures 3-1, 3-2, and 3-3. The observation cell (Number 2 in Figure 3-1, also Figure 3-3 c) is a separate component from the body of the colorimeter. It is made of Kel-F and is connected to the rest of the FIA system by stainless steel tubes that also hold it into place. It was already mentioned that the sides of the cell facing the LED and photodiode were painted black. The light path in the cell is 11.2 mm (0.44") long with an i.d. of 0.635 mm (0.025"). This gives a hold up volume of 3.54 µl. These dimensions are similar to those of the commercial cell in the detector currently used [3], which has proven to be very adequate.

The side walls of the observation cell were formed by pressing a lens and a window against the sides of the plastic cell (Figure 3-1). This design gives rise to two dead spaces to the sides of the inlet and outlet of the flow-cell (Figure 3-3 c) because these holes are not placed right at the end of the observation hole. If the inlet and outlet holes were drilled at the end of the observation hole, the area that the lens and window had to seal would be much larger, thus making the cell more subject to leakage. These dead spaces produce some problems with the flow patterns of the FIA system as discussed in the next chapter.

The body of the cell (Figure 3-2) as well as the holders for the photodiodes and LED (Figure 3-3 a, b) are made of black Delrin which prevents ambient light from reaching the photodetectors. The two holders are tightened simultaneously to balance the pressure on the lens and the window at the sides of the cell. This pressure has to be strong enough to produce a leak-proof seal, but not so excessive as to break the glass components.

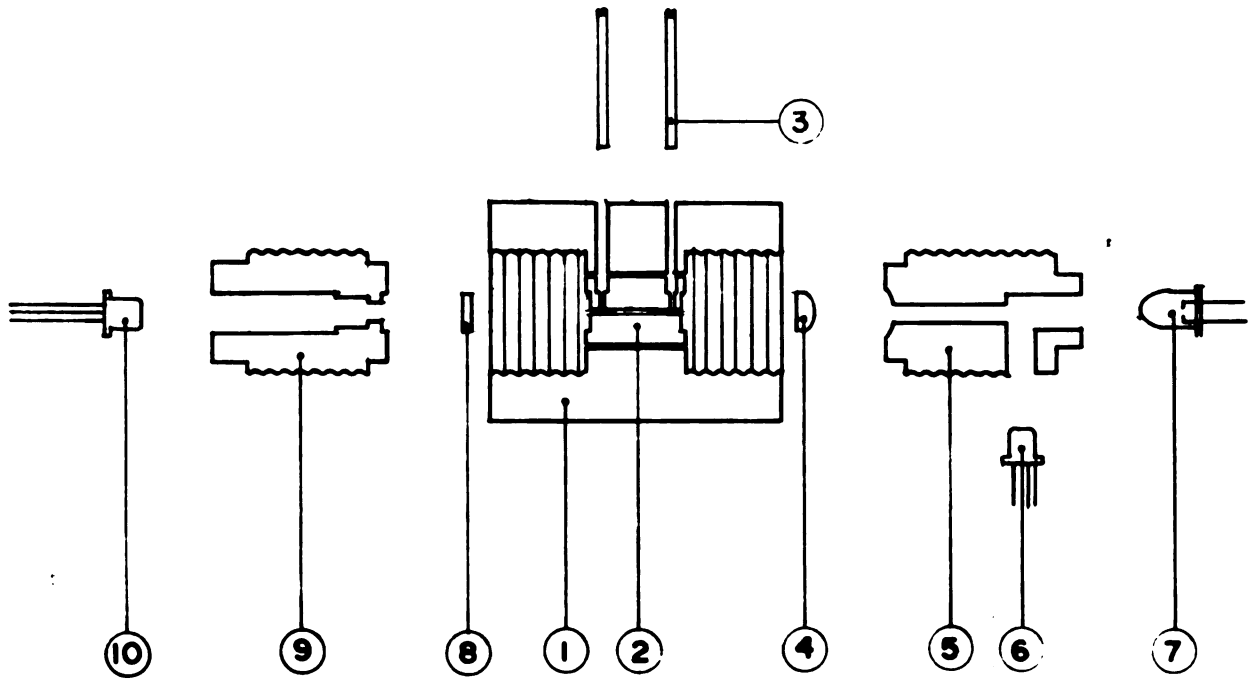

1. Cell body
2. Removable observation cell
3. Stainless steel connecting tubes
4. Lens
5. LED socket
6. Reference photodiode
7. LED
8. Glass window
9. Photodiode socket
10. Photodiode

FIGURE 3-1: Construction of the Photometric Cell used in every channel of the detector.

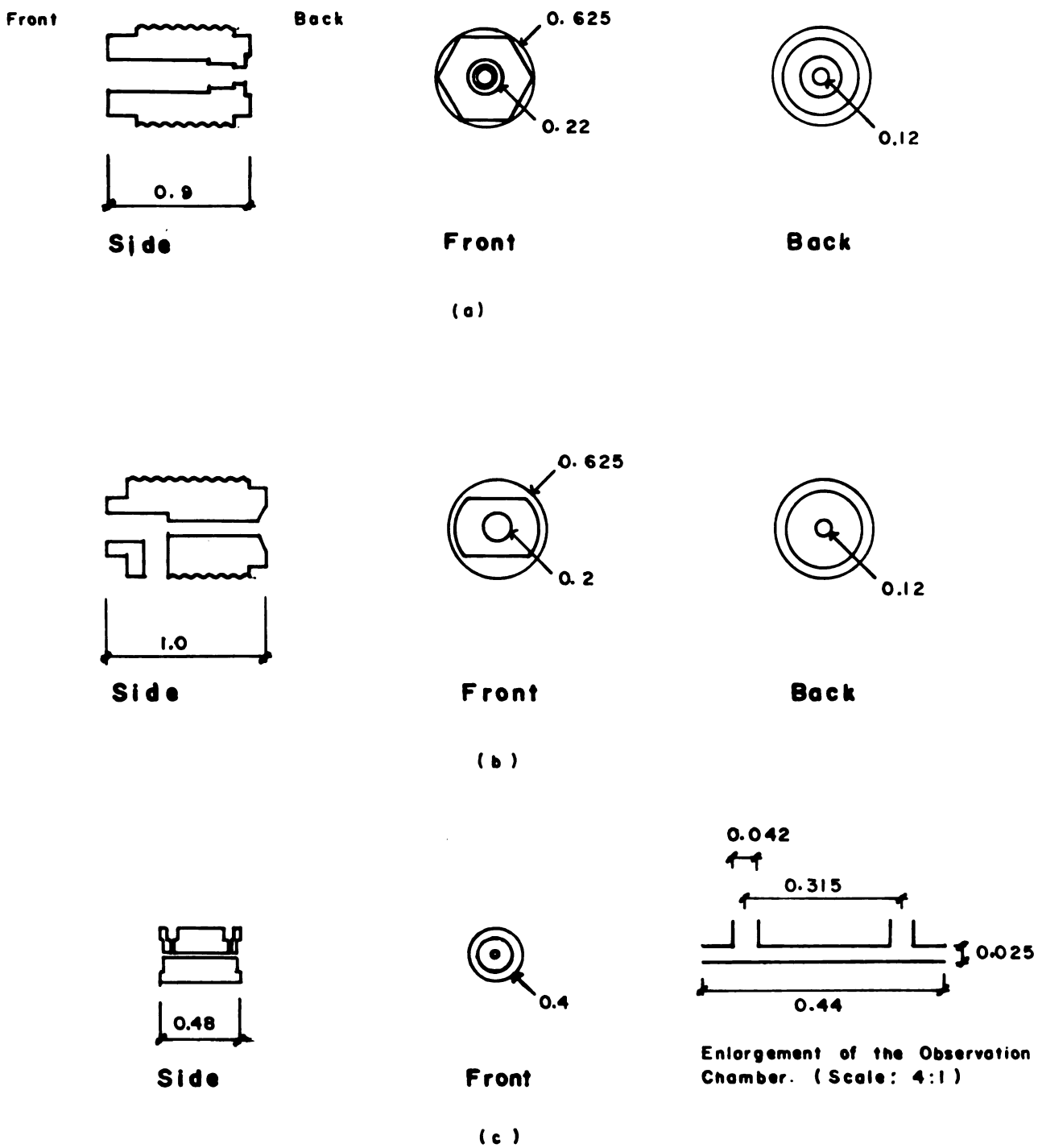

FIGURE 3-3: Other parts of the colorimeter: a) Photodiode socket (Delrin); b) LED socket (Delrin); c) Observation cell. All measurements in inches. (Drawn to scale).

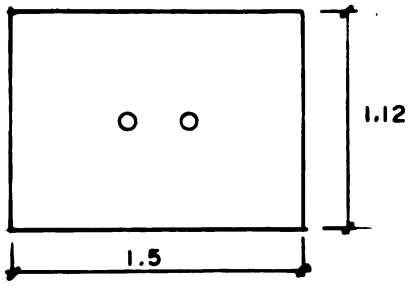

Plan

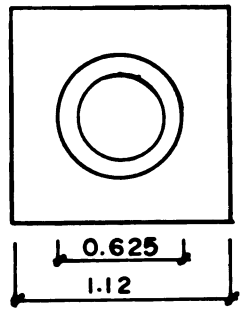

Front

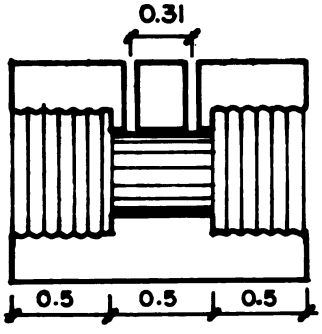

Longitudinal Section

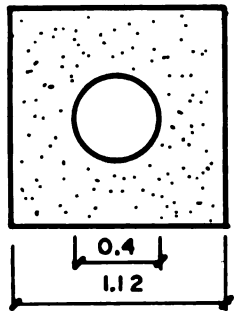

Cross Section

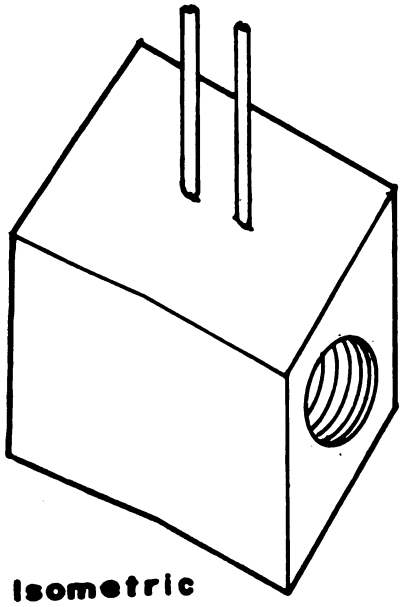

Isometric

FIGURE 3-2: Cell Body made of Delrin. All measurements in inches. (Drawn to scale)

The use of a beam splitter in the LED to produce the reference signal was avoided by placing the reference photodiode so that it views the tip of the LED. The air-plastic interface at this point scatters enough light to be detected by the photodiode to produce the reference signal that is used to control the intensity of the LED. No glue is used to hold the photodiodes and LED in place, so they can be easily removed and replaced if necessary.

3. Choice of Components

a. LED:

Several electro-optical characteristics must be taken into consideration when choosing the appropriate LED, the most important being the peak emission wavelength, which should be as close as possible to the wavelength of maximum absorptivity of the analyte. Also important is the spectral line halfwidth which will determine, among other things, the linear range of the calibration curve. The luminous intensity is an important factor to consider given the small internal diameter of the observation cell, which greatly restricts the amount of light reaching the photodetector. For the same reason, it is important to have a small beam divergence, which is measured as the "half-value" angle, the off-axis angle at which the luminous intensity is half the axial luminous intensity [36]. The last factor to be considered is the peak forward current, which is the maximum forward current that can be applied to the diode to give the highest luminous intensity without burning it.

In the enzymatic determination of sugars (see discussion on page 16), the substance to be detected, malachite green, shows a maximum absorption at 618 nm (Figure 3-4). Four types of LED's were considered

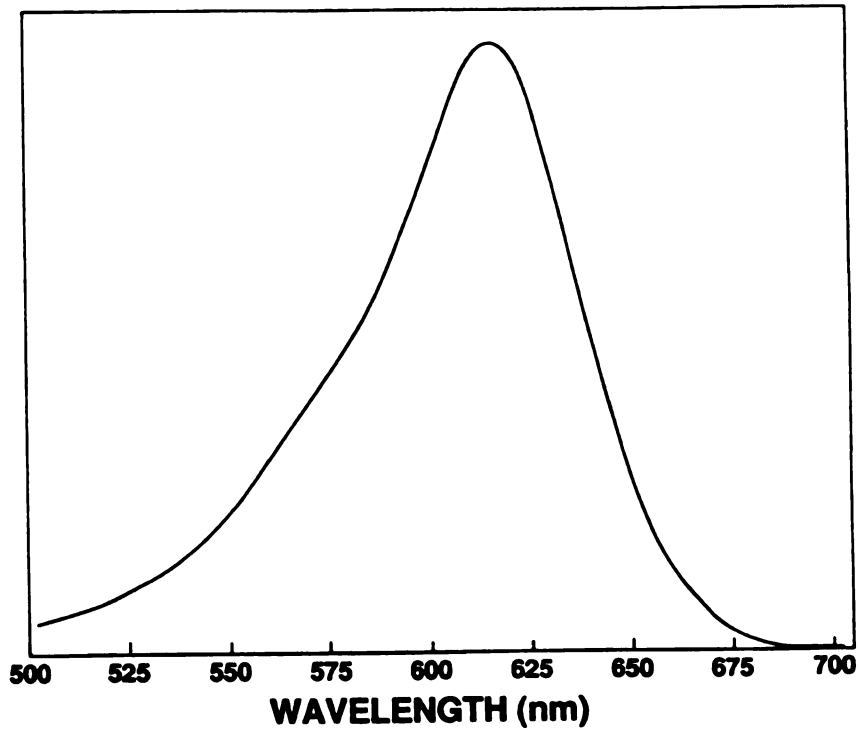

Figure 3-4: Absorption spectrum of malachite green, the substance detected in the enzymatic determination of sugars.

as possible light sources for this wavelength: two from Hewlett Packard with maxima at ≈ 585 and 640 nm (part numbers HLMP-3850 and 3750 respectively); one from Sharp Electronics Corporation with a maximum at ≈ 610 nm (part number GL5HS40); and one from Radio Shack with a maximum at ≈ 660 nm (ultra-bright type). The spectrum of the LED from Radio Shack and typical spectra from the other LED's considered are shown in Figures 3-5 and 3-6. The ultrabright LED from Radio Shack is ten times brighter than the other LED's, and the spectral line halfwidth is 15 nm narrower. It would be the first choice if the overlap with the absorption spectrum of malachite green were not so poor. Nevertheless, it was considered as a possibility for experiments in which a large linear range is required, and in which sensitivity is not critical. From the remaining three LED's, the one from Sharp had the best overlap with the absorption spectrum of malachite green, but it also showed the lowest luminous intensity.

The light throughput of the two light sources of the detectors used in the sugars analyzer were compared by measuring the photocurrent produced by the two optical systems: a miniature tungsten lamp, bifurcated fiber optic and bandpass filter, the setup in Patton's detector [3], and a LED placed right in front of the glass flowcell with a forward current of 20 mA, a setup similar to the LED detector. The LED from Sharp gave photocurrents of the same magnitude as those of the tungsten lamp setup; the photocurrents from the Hewlett Packard LED's were twice as high; and the ultrabright LED from Radio Shack gave a photocurrent too high to be measured by the detector electronics. In order to get a measurable photocurrent, the forward current for that LED had to be reduced to 3 mA.

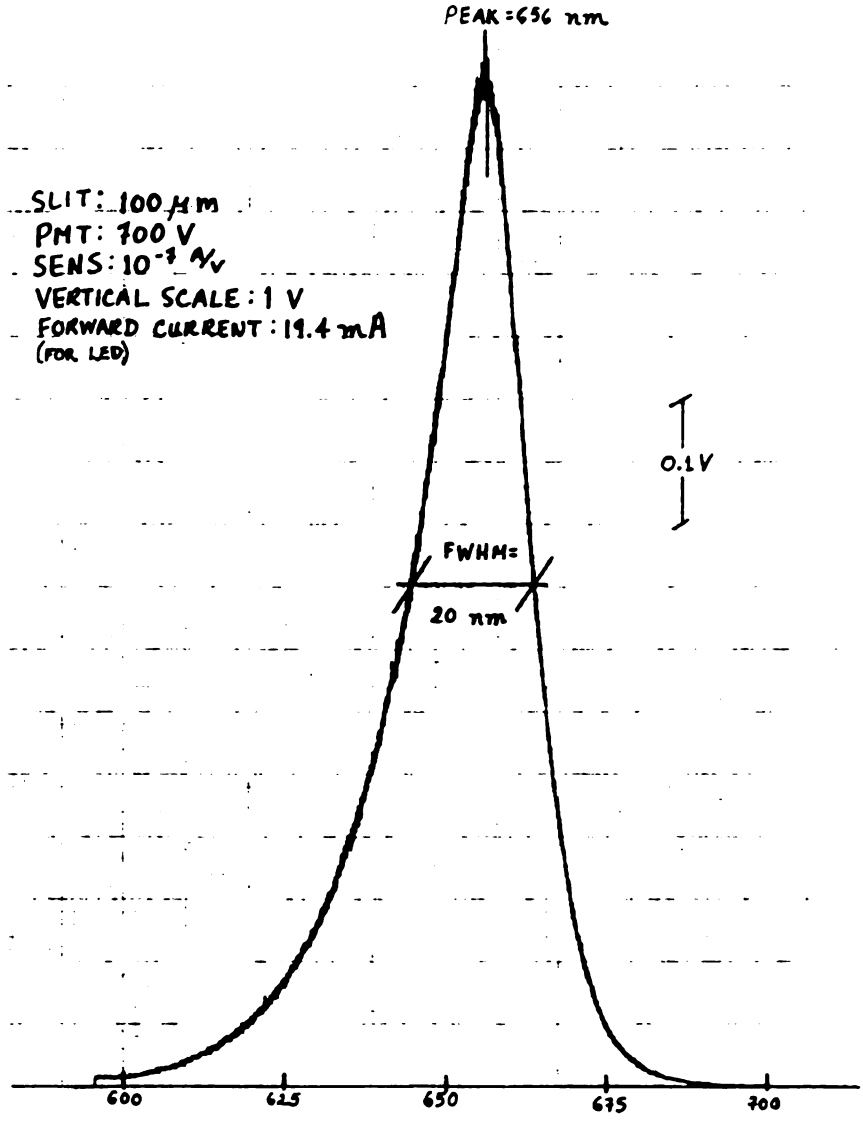

Figure 3-5: Emission spectrum of a ultrabright type LED from Radio Shack.

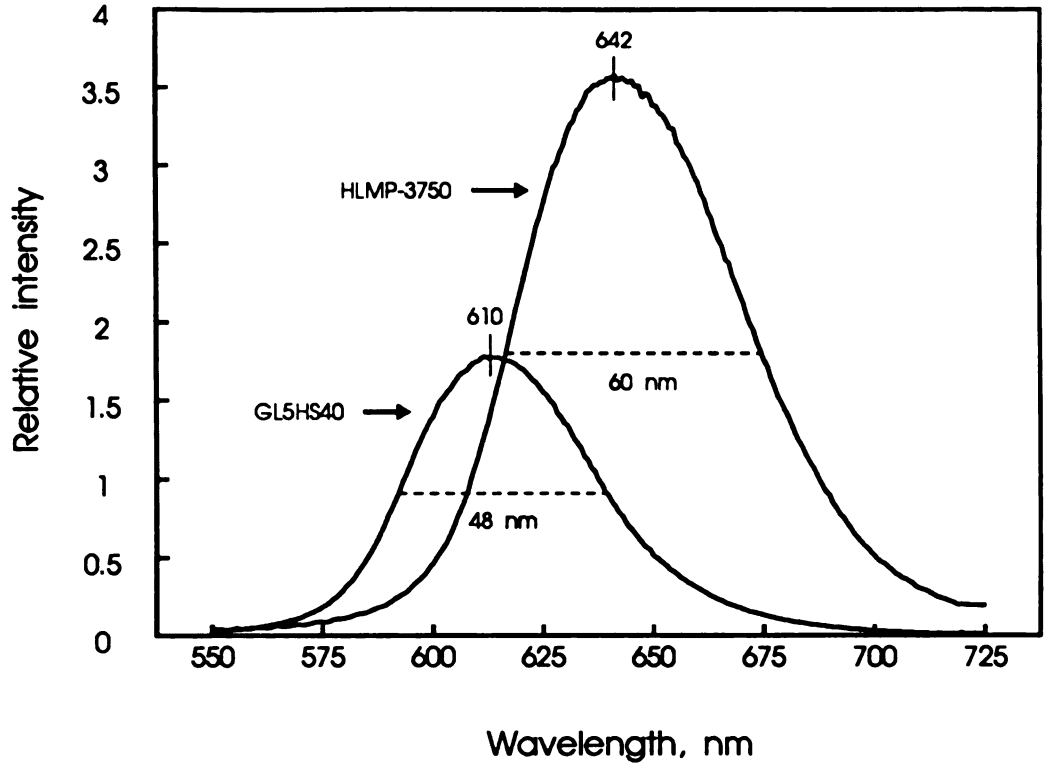

Figure 3-6: Emission spectra of two available LED's for the detection of the malachite green

b. Lens and Window:

The purpose of the lens is to concentrate the light beam that reaches the photodiode. Two different ideas were considered when choosing the lens. One possibility was to use a lens of short focal length and place the LED far enough away to simulate a collimated beam, so that the light could be focused to a point close to the end of the flow-cell. This calls for a focal length between 8 and 10 mm, which would require an impractical distance between the LED and the lens to produce a "collimated" beam. Only with very short focal lengths (around 3 mm) would that distance be reasonable. The alternative considered was to place the emission element of the LED at the focal point of the lens. Given that the LED is far from being a point source, the divergence of the beam was reduced, but good collimation was not obtained. A coated lens of 6 mm in diameter and 18 mm focal length was used. This is the distance from the lens to the LED and to the photodiode.

A glass window 6 mm in diameter and 2 mm in thickness was made for the other wall of the flow cell.

c. Photodiode:

The photodiode selected was a low bias voltage type from EG&G Photon Devices (model FFD-040B). Similar to other photodiodes available, this photodiode shows a maximum responsivity in the IR region (around 900 nm) with a spectral range from 400 to 1150 nm. The responsivity in the region of absorption of malachite green is about 70% of the maximum with a value of 0.4 A/W [37].

The photodiode has a circular active area 1 mm in diameter, which is slightly larger than the diameter of the observation cell. The smallest active area available was used to minimize the dark current when the

photodiode was operated under a bias voltage. At the end, only the reference photodiode was operated with a bias of -15 V, with the main photodiode operating in the photovoltaic mode (no bias voltage).

The first set of photodiodes received had the active area slightly off-center, but this deficiency was not observed in the second set. Photodiodes with active areas not centered were used only for the reference circuit.

B. THE SYSTEM ELECTRONICS

Each colorimeter has two independent circuits: one to control the LED and one to process the signal produced by the photodiode. The six sets of circuits operate independently of one another, and the only component shared is the reference voltage chip. A commercial power supply (Model SLD-15-808-15 from Sola) with a separate housing provides the power for all the circuits via a bus line with ±15 V and a grounded common line.

The circuitry was wired using the Scotchflex system with a punchboard.

1. Light Regulation Electronics

A diagram of the circuit that controls and regulates the light level from the LED is shown in Figure 3-7. The current from the reference photodiode is first converted to a voltage that is compared against a reference voltage. The output of this comparator controls the current driving the LED to produce a negative feedback loop that keeps the light level constant. An offset voltage is added to the summing point of the current-to-voltage converter to adjust its output, which in turn adjusts the LED current and the light level. The reference voltage used by the

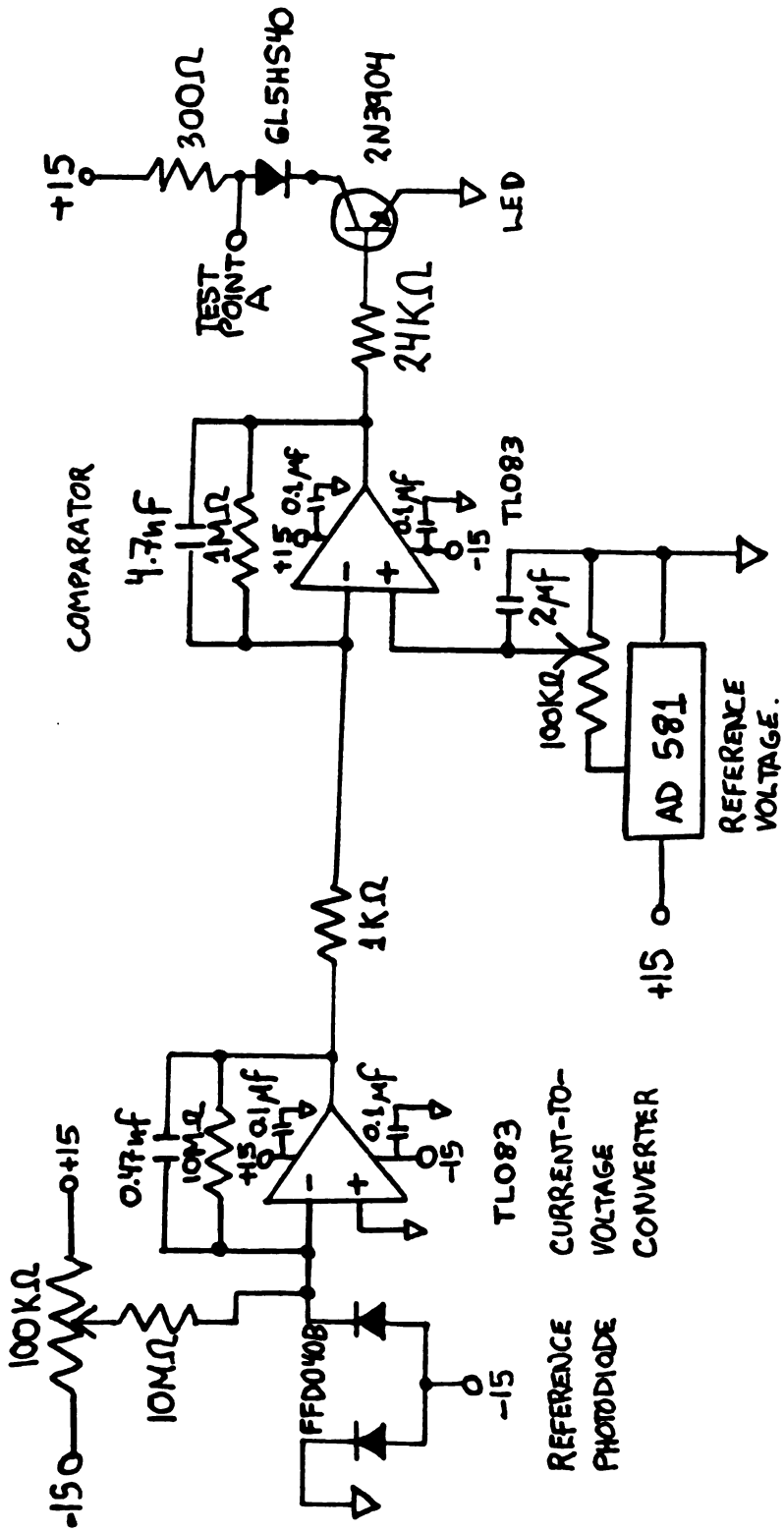

Figure 3-7 **Light regulating circuit. The current produced by the reference photodiode controls and regulates the intensity the LED.**

comparator is a fraction of the output of a 10 V constant voltage source. Adjusting this fraction also adjusts the LED current. A good way to measure this forward current is to measure the voltage drop across the resistor limiting the current (test point A in Figure 3-7). A value of 9 V at this point corresponds to a nominal current of 20 mA. A value of 6 V corresponds to the maximum current recommended (30 mA).

The reference photodiode is biased at -15 V for two reasons: the increase in photocurrent requires a smaller resistor in the current-to-voltage converter; and the output of this converter will have the correct polarity to be compared to the reference voltage, which eliminates the use of an extra component to invert the signal.

The capacitors in parallel with the resistors of the current-to-voltage converter and the comparator reduce the bandpass to 34 Hz. The capacitor in the reference voltage source gives a bandpass of 2 Hz. To measure the noise that this combination of bandpasses allows in the current of the LED, the voltage at its anode was observed with an oscilloscope. The 9 V signal showed a 60 Hz noise component of 12 mV p-p and also noise at higher frequencies up to 90 MHz with amplitudes as high as 8 mV p-p.

Each channel of the detector uses one dual op-amp chip (TL083-ACN from Texas Instruments), but the reference voltage source (Analog Devices 581) is the same for all the channels. With this set up, an increase in the reference voltage will decrease the light levels of all the channels; an increase in the offset voltage at the current-to-voltage converter of any channel will decrease the light level of that channel only. This is an important feature that allows the operator to set all the channels to the same output voltage, since individual photometric cells

have different light throughput due to small differences in construction, and different LED's require different currents to provide the same luminous intensities. Also, in a specific determination, the working range of any channel can be increased if needed by increasing its light level individually.

2. Signal Processing Electronics

The diagram of this circuit is shown in Figure 3-8. It consists of a very sensitive current-to-voltage converter followed by a variable gain amplifier. In this circuit the photodiode is used with no bias voltage to minimize the dark current.

A high quality operational amplifier (OP-43EJ, Precision Monolithics Inc.) is used for the current-to-voltage converter. This op amp combines a low bias current (5 pA max.) with a low offset voltage (0.25 mV max.). A large resistor in the feedback loop was avoided by using a combination of resistors that gives a high equivalent resistor to the converter. The transfer function of the converter is 5.1×10^8 V/A. The capacitor in parallel reduces the bandpass to 16 Hz.

The current-to-voltage converter is enclosed in an aluminum shielded box (Pomona Electronics) to eliminate oscillations observed in the output at gains of 10 or higher. The frequency of the oscillation observed was of 120 Hz at a gain of 10 and decreased with increasing gain. The dependence of the oscillation on the gain suggested that the amplifier circuit was sending some kind of positive feedback signal to the converter. Besides eliminating the oscillation described, the shielding of the converter also helped decrease the level of 60 Hz noise.

The variable gain amplifier uses a potentiometer that can be adjusted externally. It gives a gain from 1 to 60, and the capacitor in

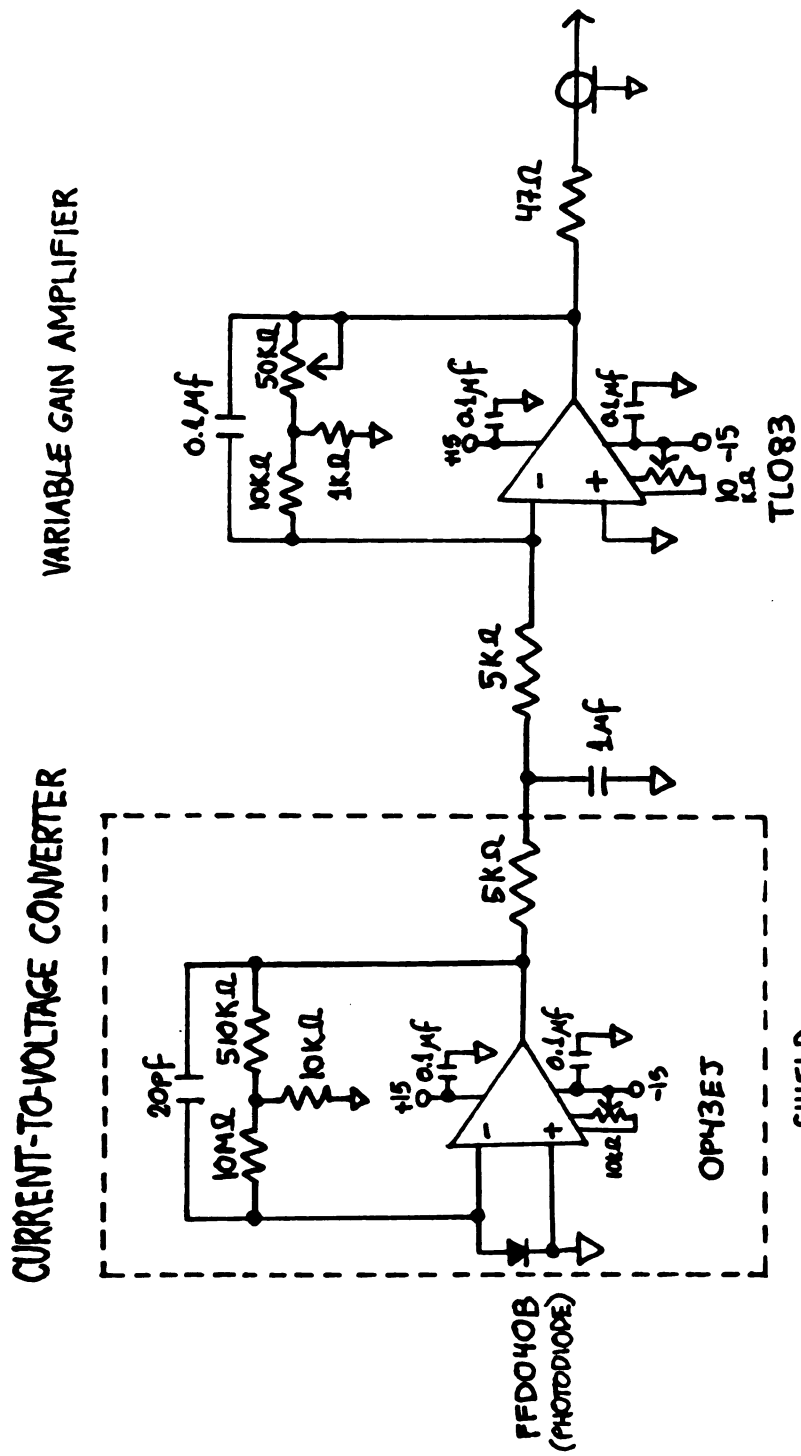

Figure 3-8 Signal processing circuit.

parallel reduces the bandpass as the gain is increased from a maximum of 159 Hz to a minimum of 3 Hz at the highest gain. This keeps the 60 Hz noise to a maximum of 6 mV p-p with output signals of 10 V. The output signal also shows noise at higher frequencies starting at 90 Hz and going as high as 90 MHz. The levels of noise from these sources are lower than 2 mV.

At low gains, the response speed of the circuit is limited by the current-to-voltage converter. At gains of about 12, the response time starts to be determined by the amplification stage, but even at the highest gain, the bandpass is high enough (3 Hz) to fully characterize any FIA peak, a signal of less than 0.1 Hz.

CHAPTER IV

OPERATION AND CHARACTERIZATION OF THE DETECTOR

This chapter begins with a description of two procedures related to the operation of the detector. The first one is the starting procedure that is followed each time the detector is used after a long period of inoperation. The second one is a less routine procedure: that of adjusting the light levels of the different photometers.

The second section of Chapter IV describes the results of various tests performed on the detector in order to form an idea of the instrument's characteristics. These tests were also applied to the detector currently used [4] in the sugars analyzer to provide a point of comparison. This detector has given excellent results, so it is a good standard against which the new detector may be compared.

The chapter ends with the results of a real glucose determination, again using both detectors.

A. OPERATION PROCEDURES

1. Initial Operation:

When the detector is used for the first time during the day, the normal warm-up period of 15 minutes for the electronics should be

allowed. It was found that after a long time of inoperation the light throughput of the flowcell is greatly reduced when the cell is stored with water, thus giving a very low signal. The signal level starts to increase when the cell is flushed with fresh water. This continues for a period of approximately 15 minutes after which the signal reaches a stable point. The initial reduction in signal is attributed to some deposition of minerals on the surfaces of the cell including the lens and the window. The time needed to wash off these residues is greatly increased because of the geometry of the cell which has dead spaces at the sides of the inlet and outlet holes (see Figure 3-3). The flow inside the cell is apparently not turbulent enough to reach these points effectively.

If, on the other hand, the cell is rinsed with plenty of distilled water after use and stored with no water, the remaining drops inside the cell evaporate. The signal in the dry cell is very strong, about 5 times stronger than the signal of the cell with water running through it; nevertheless, the light intensity drops immediately when the liquid begins to flow. When this is the case, the signal takes about 10 minutes to stabilize.

The procedure recommended, then, is to rinse the cell with distilled water after use, but to empty the cell for storage. The first time it is used after storage, the system should be warmed up for 15 minutes with water flowing through the cell.

2. Adjusting the Light Level:

As mentioned in the previous chapter, there are two controls that affect the light levels of the photometers. The reference voltage level changes the current in all the LED's simultaneously. In addition, each

channel has an individual control to adjust the current driving its particular LED.

There are two modes of operating the six photometers simultaneously. One is to adjust all the currents for the different LED's to the same value and to use the different gain controls to balance all the output levels. To set this constant current mode, the offset voltage of every channel has to be set by adjusting the corresponding trimmer to a value that gives the same current for all the LED's (the same voltage at each test point A in Figure 3-7). Once the currents are all equal, they can be brought back to 20 mA (or higher) by adjusting the reference voltage level. This mode has the disadvantage of giving a lower signal-to-noise ratio for the channels with less light reaching the photodiodes.

The second mode of operation is to adjust the forward currents of each channel in order to equalize all the output signals. The offset controls should be adjusted to give the same output levels when the gain is the same for every channel. Again, the reference voltage is used to bring back the currents to a value of approximately 20 mA. In this constant signal mode some LED's will have higher forward currents, and will thus result in slightly broader peaks and shorter lifetimes. As will be seen later, the dependency of the FWHM of the LED's emission spectrum on the forward current is very small; also, the price of the LED's is so low that replacing them more frequently would not substantially increase the price of operation of the detector. These considerations indicate that operating the detector in the constant signal mode should give better results for most applications.

It is important to remember that whenever an adjustment is being made to the light level of any channel, the forward current of the LED should be monitored in order to avoid values over the maximum rating of 30 mA (a minimum of 6 V at test point A in Figure 3-7).

B. CHARACTERISTICS OF THE DETECTOR

In order to determine the different figures of merit for the new detector, a series of measurements and experiments were performed using a single channel of the instrument (later referred to as LED-detector). The same experiments were performed with the detector constructed by Patton and Crouch [33], (later referred to as Patton's detector). Except for the experiments with methylene blue, the results presented in this section were obtained using the FIA manifold shown in Figure 4-1. This arrangement is equivalent to a single channel of the sugars analyzer depicted in Figure 2-1.

The FIA apparatus consisted of a 12-channel peristaltic pump (Ismatec model 7618-50; Glattbrugg, Switzerland) with flow-rated pump tubing (Technicon Instruments; Tarrytown, NY); a pneumatically activated injection valve (Rheodyne Inc.; Cotati, CA); either a digital multi-meter (Fluke model 8000A; John Fluke MFG. Co. Inc., Seattle, WA) or a strip chart recorder for the repeatability experiments (Model SR-255 A/B, Heath Company); an IBM PC compatible microcomputer equipped with an RTI-815 interface board (Analog Devices; Norwood, MA). The computer controlled the sample injection and data acquisition via software previously written for the FIA system. Transmittance values were recorded by the computer, and the corresponding absorbance was calculated from the 100% transmittance reading. Teflon tubing of 0.86 mm i.d. (Benton-Dickinson; Parsipanny, NJ) was used throughout the

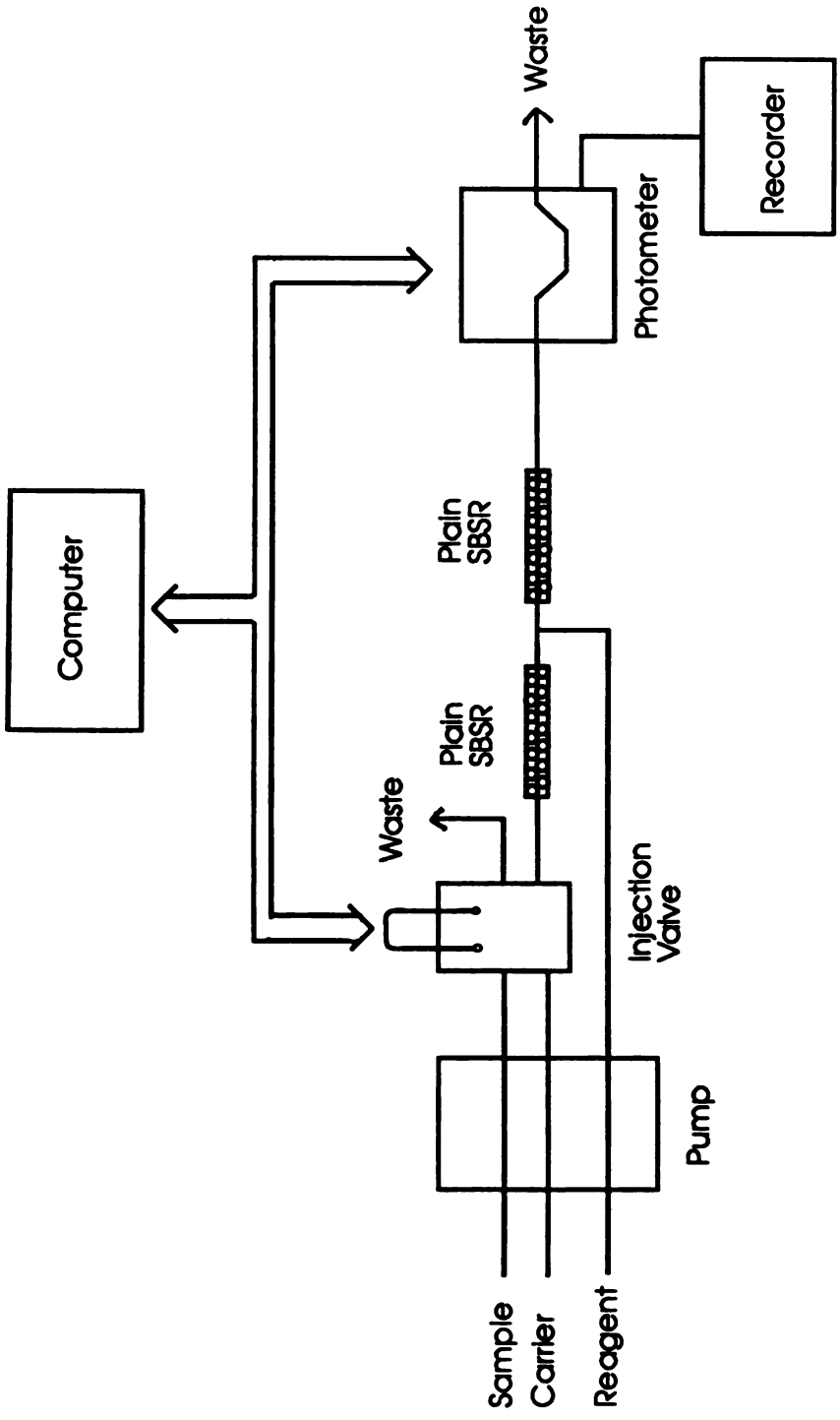

Figure 4-1: Schematic diagram of the FIA manifold used in the experiments to characterize the multichannel detector

manifold. The single bead string reactors (SBSR) were previously prepared using 0.6 mm diameter non-porous glass beads (Propper MFG. Co.; L.I. City, NY).

1. Sensitivity to Flow Variations:

The photometers of the LED-detector show an unusual sensitivity to any disturbance in the flow pattern of the liquid under observation. The oscillations of the peristaltic pump are especially problematic. The FIA peak in Figure 4-2 shows the extent of this noise. The noise frequency depends on the flow rate setting of the pump, and is generally quite low (between 1 and 3 Hz). Experiments showed that the noise increases with increasing pressure of the pump rollers on the plastic tubing. Increasing the LED brightness also increases the noise.

The shape of the peak generated by the detector response to the oscillations of the pump (as observed with an oscilloscope) suggests that it is caused by a refractive index effect also observed in the detector designed by Betteridge et al. [24], and more recently described in detail by Evans et al. [38]. This effect makes the flowing stream behave like a dynamic lens that first focuses and then diverges the light beam. The pressing action of the pump's rollers on the tubing would seem to create regions of higher and lower pressure within the stream, which may change the refractive index of the liquid just enough to produce the observed response.

The frequency of the pump oscillations is too low to be effectively filtered without affecting the sensitivity to the FIA peak. Possible ways of reducing the noise include the use of a different pump. The pump currently used in the sugars analyzer is relatively new and produces very intense oscillations. Tests with older pumps showed that as the pump

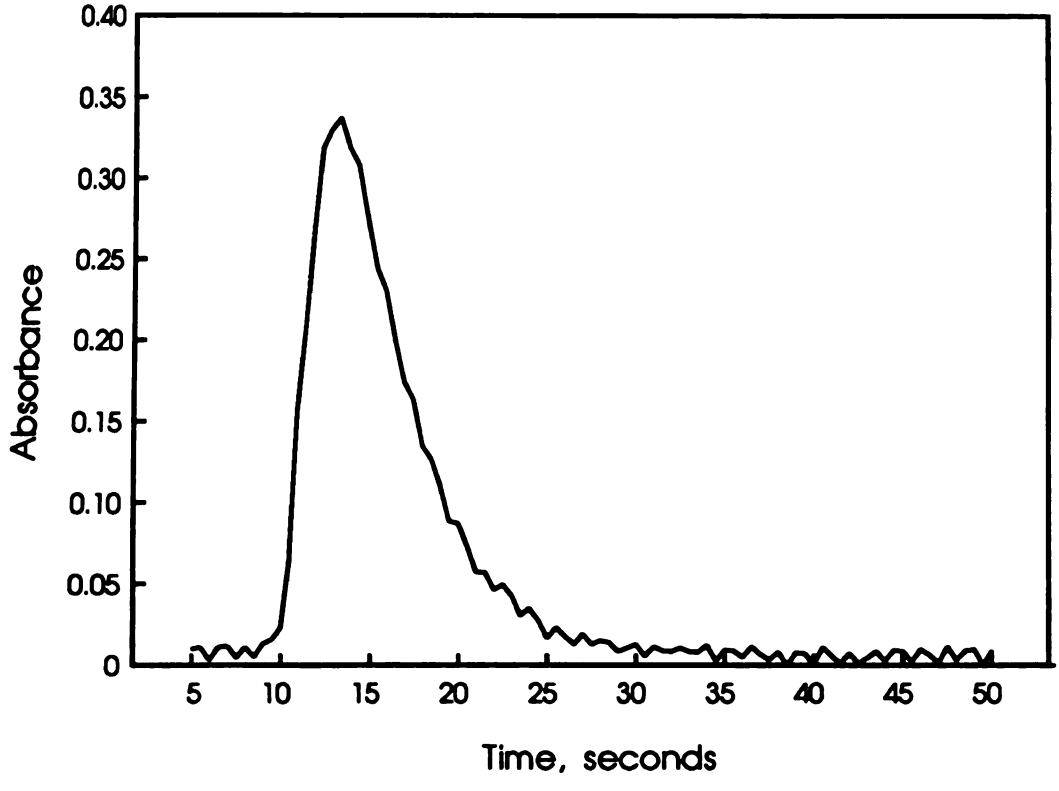

Figure 4-2: Injection of a 0.04 mM solution of hydrogen peroxide. The noise in the signal came from the pump oscillation. The flow rate was 1.3 ml/min.

gets older, the pressure exerted by the rollers is decreased, which decreases the noise in the detector signal. Using compressed gas [39] or even gravity to pump the liquid produces a completely pulse-free flow, but the compressed gas set-up is clumsy, and the use of gravity might not provide enough pressure to push the liquid through string bead or packed bed reactors. Still, these options may be implemented in extreme cases. If a peristaltic pump is to be used, a pulse dampener should be placed immediately after the pump. The bead reactors are in fact pulse dampeners, but they did not reduce the pulsations effectively, unless they were impractically long. A small stabilization device reported by Bergamin et al. [40] (Figure 4-3) proved to be effective in reducing the pulsations when placed right after the pump in the carrier channel. The addition of one of these devices to the sample or reagent channel did not reduce the noise, however, and produced an unwanted peak caused by the sudden change in pressure during the injection process (Figure 4-4).

A problem with using a pulse dampener like the one described above arises when the flowing liquid is changed, for example, from water to a reagent. Every time the glass bulb is emptied and filled with a new liquid, the baseline at the output takes about 15 minutes to stabilize. This of course represents a longer waiting period and some waste of reagent. With our particular sugars analyzer, however, the reagents are never changed, so this process would have to be carried out only when the detector is used with water before the experiments are run on a given day. This can be avoided if the same carrier that will be used in the experiment is used in the initial stabilization period.

The question remains of why the detector is so sensitive to the small changes in the refractive index of the flowing liquid. Reports on

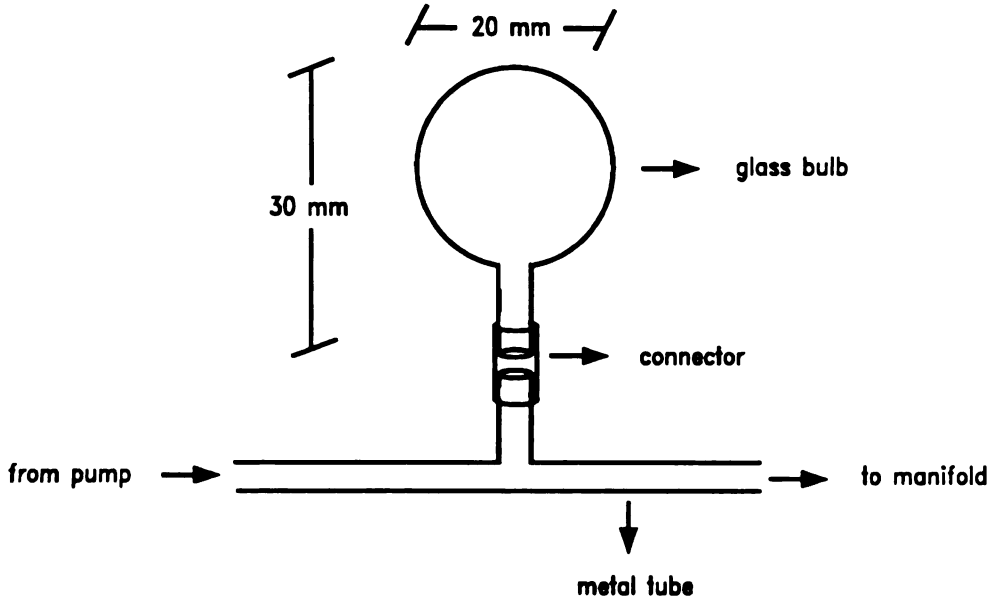

Figure 4-3: Stabilization device used in the carrier channel after the pump to reduce the effect of its oscillations.

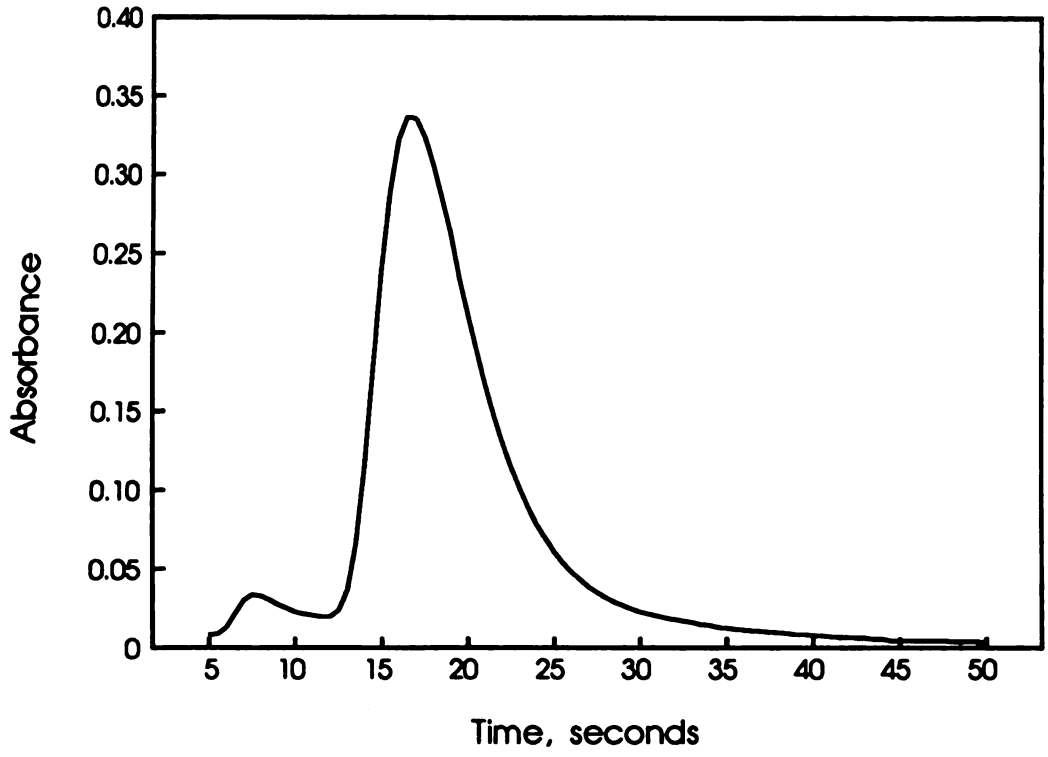

Figure 4-4: Injection of a 0.04 mM solution of hydrogen peroxide using two stabilization devices: one in the carrier channel and one in the sample channel. The small peak at 8 seconds was caused by the injection process.

other photometric detectors for FIA, including the detector currently used in the sugars analyzer, have not mentioned such a high sensitivity to changes in the refractive index of the observed liquid. Three causes are suggested: 1) the very small internal diameter of the flow cell (all other LED-based detectors had cell dimensions at least twice as big as those in the multichannel detector); 2) the position of the lens and window might not be exactly parallel due to uneven pressure from the holders (this would change the angle of incidence of the beam); and 3) the active area of the photodiode is too small (if the active area is much larger than the aperture stop defined by the internal diameter of the flow cell, the dynamic lens effect is minimized).

To further study the first suggested cause for the problem, a new observation cell was constructed with a larger internal diameter (1.5 mm instead of 0.6 mm). The peaks produced by this cell (Figure 4-5) did not show any reduction in the baseline pulsations. In fact, these pulsations were increased to the point that the pulse dampener was not able to completely eliminate them (Figure 4-6). Also, the bigger cell produced longer elution times. This is expected since the cell's internal diameter is almost twice as large as the rest of the FIA tubing used.

No further attempts were made to reduce the detector's sensitivity to flow variations, since the pulse dampener placed in the carrier channel gave excellent results. All the experiments reported in the following sections were run using this device.

2. Baseline Noise and Drift:

The baseline electrical noise was measured with the aid of an oscilloscope. Two different types of noise were observed. One type is due to oscillations from the peristaltic pump. These oscillations were greatly

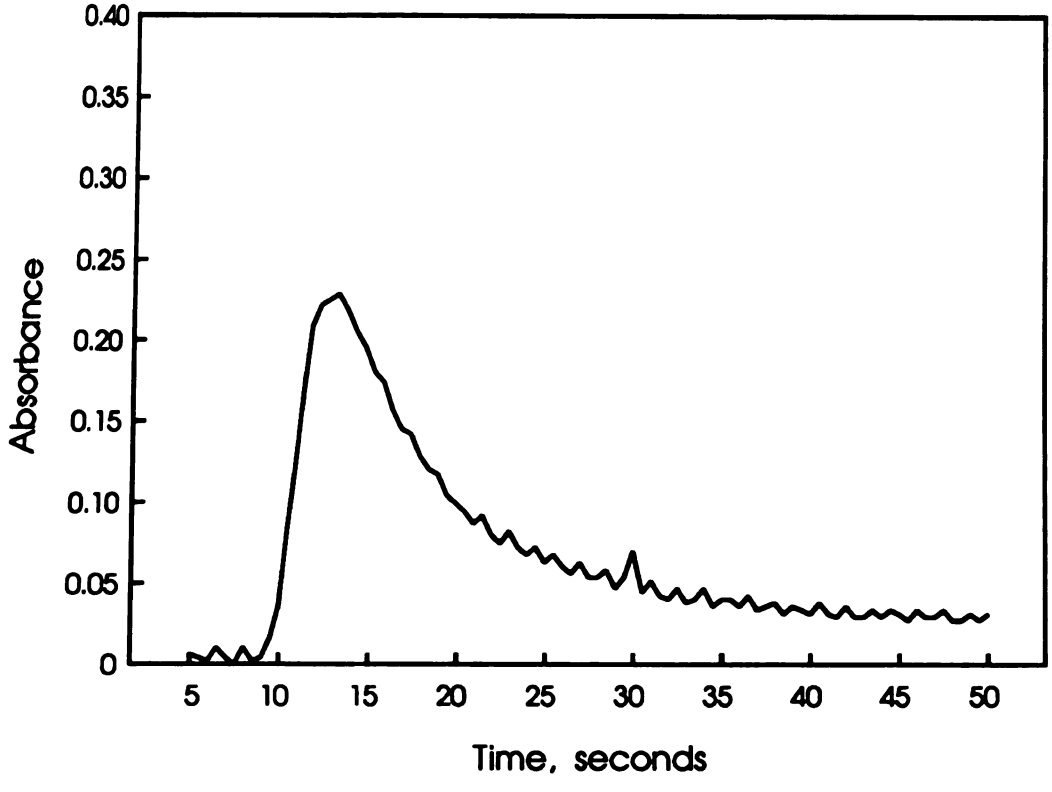

Figure 4-5: Injection of a 0.04 mM solution of hydrogen peroxide using a larger observation cell. The noise in the signal came from the pump oscillation. The flow rate was 1.3 ml/min.

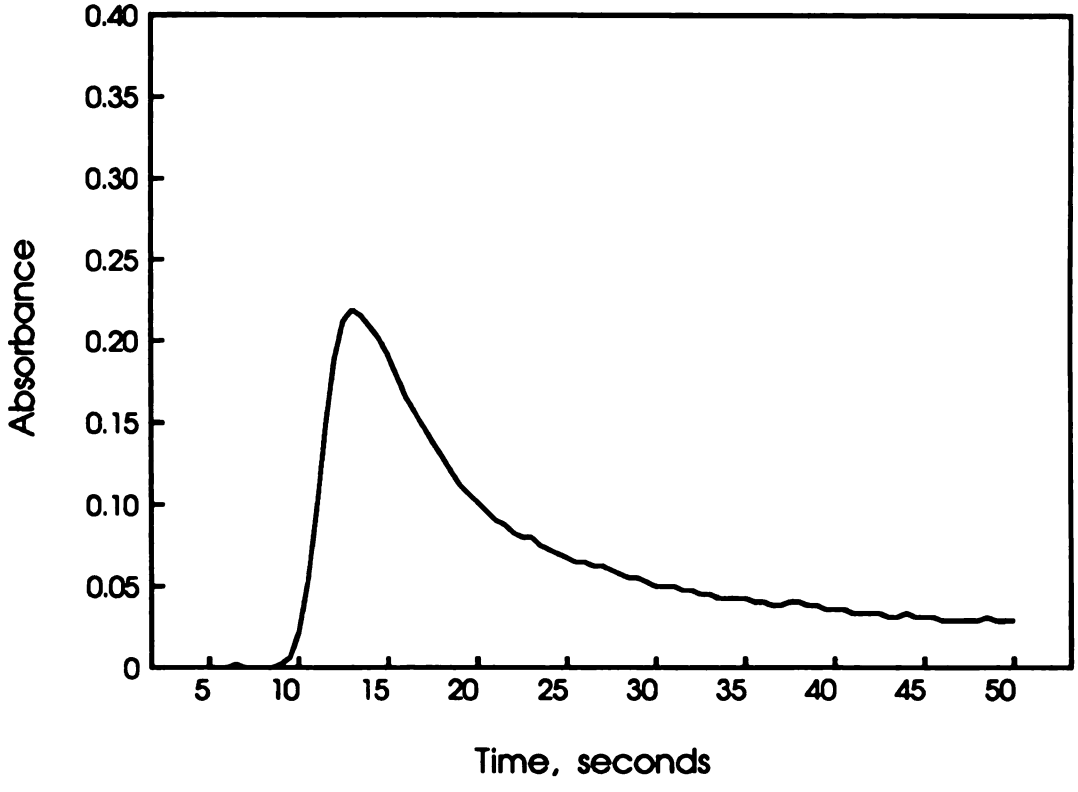

Figure 4-6: Injection of a 0.04 mM solution of hydrogen peroxide using a larger observation cell and one stabilization device in the carrier channel.

decreased by the use of the pulse dampener, but not totally eliminated. Because of its low frequency, this noise cannot be effectively reduced by the RC filter of the variable gain amplifier, and its amplitude increases with increasing gain. At the minimum gain the noise can hardly be detected, but at the gain needed to reach an output of 5 V (approximately 10) it has an amplitude of 10 mV. This represents a baseline noise of 0.001 Absorbance Units (A.U.) near zero absorbance.

The second type of baseline noise comes from the ac power line. Noise at 60 and 90 Hz and higher harmonics is present with an amplitude lower than the pump noise. This fixed-frequency electrical noise is effectively filtered at higher gains so that the amplitude remains approximately constant. The 60 Hz noise was about 6 mV p-p and the higher frequency noise was 2 mV p-p or less.

Three different types of drifts in the baseline can be defined. The first drift is due to the electronics. This was measured with no liquid flowing through the cell and monitoring the output with the aid of a chart recorder. A drift of 0.001 A.U./hr. was observed. A much higher drift was observed when there was liquid flowing through the cell, especially when the cell was used for the first time during the day, as previously explained. It was suggested that a 15 minute period of conditioning the cell with the reagents flowing was enough to obtain a reasonable drift. Under these conditions the measured drift is 0.002 A.U./min, normally increasing the baseline signal, a fairly high value but still low enough to accurately record an FIA peak (which takes less than one minute to go from baseline to maximum). After one hour of operation the initial drift due to the flow was reduced to 0.001 A.U./min. This third type of drift was observed in both directions —decreasing or

increasing the baseline signal— and it was also observed in the tests with Patton's detector. The drift may be caused by very small variations in flow rates, probably due to small variations in the voltage supplied to the pump.

3. Peak Broadening:

There are three factors that contribute to the broadening of the peak produced by a flow-through detector [41]: 1) dispersion in the connecting tubes; 2) a finite effective measuring volume; and 3) the dynamic behavior of the transducer and signal processing electronics. The first factor seemed to be negligible for the LED detector since the connecting tubes are less than 2 inches long. Nevertheless, it was observed that the peaks recorded with the LED detector had a delay of about 0.6 seconds with respect to the peaks recorded with Patton's detector (Figure 4-7). This is a result of the liquid having to travel a longer distance through the connecting tubes. It can also be observed in Figure 4-7 that the peaks of the LED detector do not fall as fast as those obtained with Patton's detector. This higher dispersion of the LED detector is produced in part by the effect of the laminar flow in the open connecting tubes. There should also be a contribution from the second factor mentioned above, that is, the cell in the LED detector must behave more like a mixing chamber than the cell in Patton's detector. This is expected since the drilled plastic walls in the LED cell must have a more uneven surface than the glass ones in Patton's commercial cell. To estimate the contribution to dispersion from the second factor, we can assume that the flow cell in the LED detector behaves completely as a small mixing chamber (the worst case). Then, the volume standard deviation is the cell volume V_C, and the time standard deviation from this

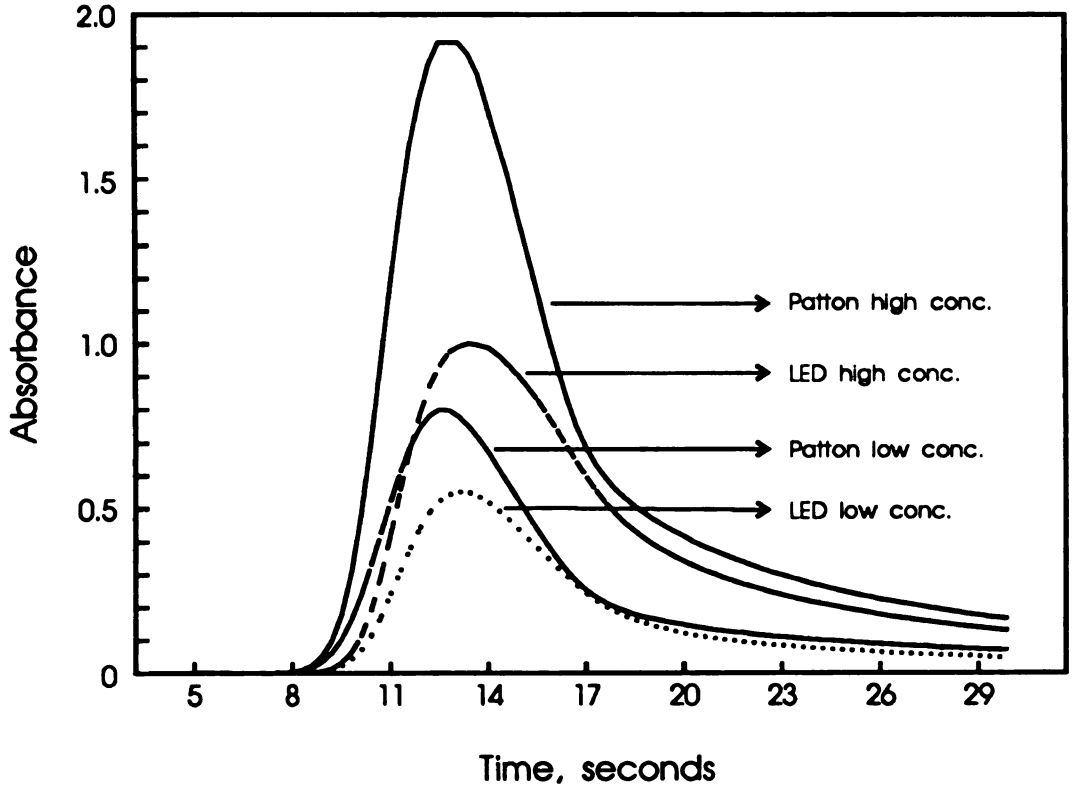

Figure 4-7: **Dispersion patterns for both detectors at low and high sample concentrations.**

factor is the cell volume divided by the flow rate, $\sigma_t = V_c/f_r$. For a typical glucose determination, the total flow rate is set at around 9 μL/s; the LED photometer has an observation cell with a measuring volume of 3.54 μL. This gives a peak broadening due to the cell volume of 0.40 s. The contribution of the third factor can be estimated from the time constants in the amplifier chain. With a typical gain value of 10, the time constant of the I/V converter is of the same magnitude as the one from the amplifier: 10 ms. This would give a total contribution of 14 ms, which is negligible compared to the contribution of the other two factors.

In the determinations done with the multichannel detector, typical peak widths were on the order of 20 s. Following the guidelines given by Ruzicka and Hansen [7] the detector should contribute a maximum of 5% to the overall peak width. This permits a contribution from the detector up to 1 s. Even with the increased dispersion, the LED detector still falls within the recommended limits set by the FIA system as used in the sugars analyzer.

4. Dynamic Range:

The main objective of the experiments done in this area was to determine the photometric working range for the LED detector and the linear part of that working range. Possible factors affecting the deviation from linearity were also studied.

Four major factors were seen to contribute to deviations from linearity: two coming from the detector: stray light and non-monochromatic light; one coming from the FIA manifold: insufficient dispersion of concentrated samples; and one from the chemical system: the detection reaction in the sugars determination is an equilibrium one.

The following experiments give some guidelines to understand the effect of these factors.

a. Experiment 1: Calibration curve using LMG-H_2O_2. Solutions of different concentrations of H_2O_2 were used to study the detection reaction for the enzymatic determination of sugars. The procedure is the one suggested by Aspris [6] and Kurtz [5]. The stock solutions needed for the experiment were: Hydrogen Peroxide 0.01 M to prepare the different samples of concentrations 0.02 to 0.20 mM; Leucomalachite Green (LMG) 0.5 g/L (1.5 mM) in Acetic acid 37%; phosphate buffer (0.1 M, pH 6); and acetate buffer (0.1 M, pH 4). The reagent solution was prepared by dissolving 8 mg of horseradish peroxidase in 2.4 ml of pH 6 buffer, adding 0.6 ml of stock LMG, and diluting to 10 ml with pH 4 buffer. The final concentration of LMG in this solution is 0.090 mM. This solution had to be prepared just before the determination as it is unstable to light and atmospheric oxygen. The phosphate buffer pH 6 was used as a carrier and also to prepare all the H_2O_2 solutions. The flow rates in the carrier, sample, and reagent channels were 0.51, 0.40, and 0.06 ml/min respectively (pump setting of 30). A 30 µL sample was injected, each sample being injected in triplicate for this and the rest of the experiments. A 10 cm plain SBSR was used in place of the glucose oxidase reactor, and a 30 cm plain SBSR was used for the detection reaction. Patton's detector was used with a filter centered at 620 and a bandpass of 20 nm. The LED detector was used with the LED from Sharp Electronics emitting at 610 nm and with a forward current of 30 mA.

The results are presented in Figure 4-8. The curves for both detectors show the same tendency to level off at absorbances of 0.75 for

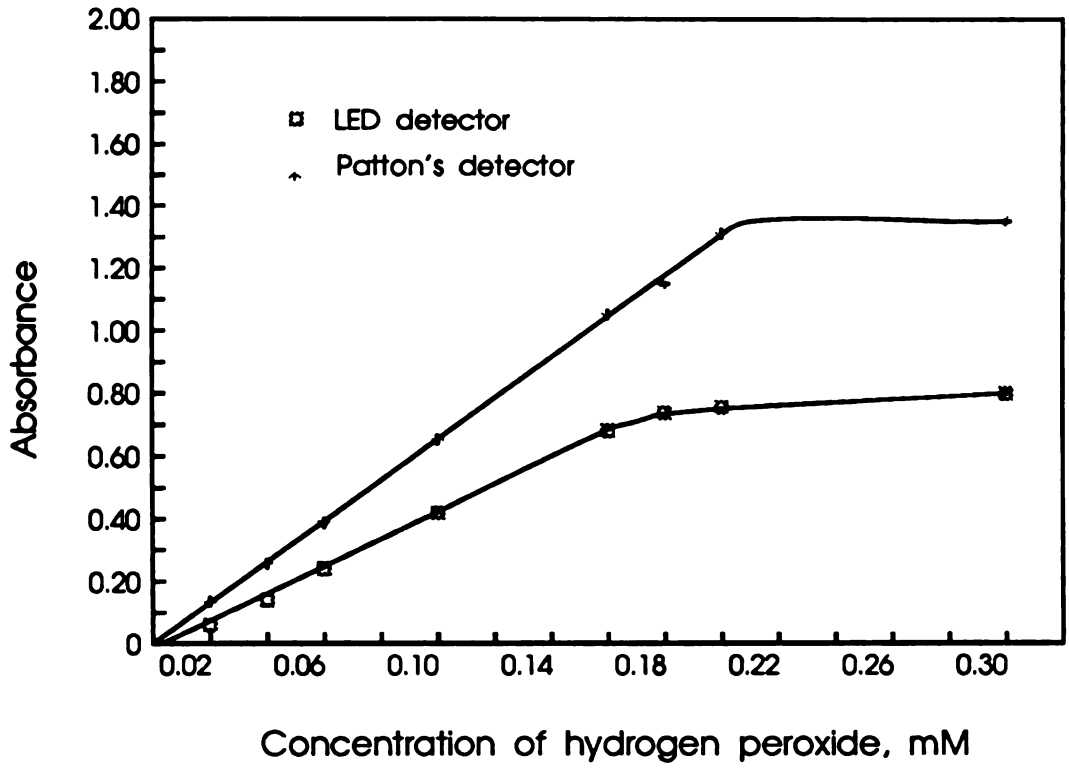

Figure 4-8: Calibration curve using LMG-hydrogen peroxide with stock solution of LMG 1.5 mM.

the LED detector and 1.3 for Patton's detector. The deviation from linearity in both cases starts at concentrations above 0.16 mM. The slopes of the linear ranges are: Patton detector, 6.56 A/mM; LED detector, 4.28 A/mM. The response of the first detector is 1.5 times higher than that of the second one. The similar behavior in the curves from both detectors suggests that the reagent LMG might be limiting the reaction at concentrations of H_2O_2 above 0.16 mM. This is very possible since the effective concentration of LMG in the carrier stream is 0.010 mM.

b. Experiment 2: Effect of the concentration of LMG. The same experiment is repeated keeping all the conditions constant but increasing the concentration of the stock solution of LMG to 1 g/l (3 mM). This gives a final concentration of LMG in the reagent solution of 0.180 mM. The problem with increasing the concentration of LMG in the reagent solution is that its instability increases, so the solution has a shorter usable period of time. The standard solutions of H_2O_2 are prepared from 0.05 mM to 0.40 mM to have a wider range of observation.

The results of this experiment are shown in Figure 4-9. The general shape of the curves is similar the curves in Figure 4-8, with two important differences: The deviations from linearity now start at higher concentrations (above 0.25 mM); and the values of absorbances where the curves level off are consequently higher. The slopes for the linear part of the curves are: Patton's, 7.36 A/mM; LED's, 3.82 A/mM. The possibility of a limiting reagent is still present since doubling the concentration of reagent roughly doubled the concentration of H_2O_2 where the deviation started. Of course, there is also the possibility of other factors affecting the curves, since there were high concentrations of

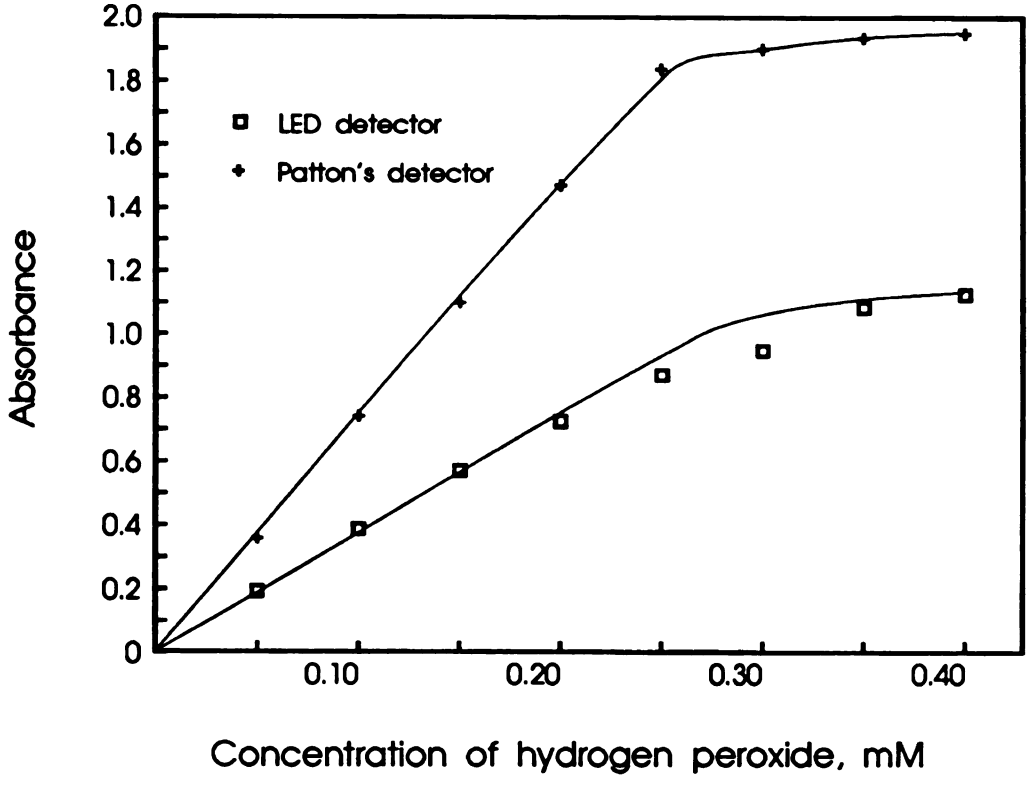

Figure 4-9: **Calibration curve using LMG-hydrogen peroxide with stock solution of LMG 3.0 mM.**

H_2O_2 involved and high absorbance values, at least in the case of Patton's detector.

c. Experiment 3: Effect of the light throughput and stray light. The conditions in experiment 2 were used to compare the performance of two observation cells of different diameters in the LED detector. If the observed deviations from linearity were caused by stray light, increasing the light throughput in the observation cell should decrease the percentage of stray light reaching the photodiode. A regular diameter cell (0.6 mm) and a large diameter cell (1.5 mm) were used with the added feature of having the side walls of the cells facing the LED and the photodiode covered with a sealant and painted completely black to block any possible stray light.

The results are presented in Figure 4-10. The two calibration curves are practically the same as the ones presented in Figure 4-9 for the LED detector. The slopes for the linear part of the curves are: large cell, 4.31 A/mM; small cell, 3.92 A/mM (compare to 3.82 A/mM for this cell in the previous experiment). The efforts to reduce the stray light in the LED detector did not improve its response. The effect of increasing the amount of light reaching the photodiode through the observation cell had little effect on the general shape of the calibration curve.

d. Experiment 4: Effect of the concentration of LMG. The conditions of the detection reaction were completely changed to try to improve the working range. The new conditions were: stock solution of LMG 3 g/l (9 mM) in acetic acid 37%; and phosphate buffer (0.05 M, pH 6.86) used to prepare the reagent solution, the H_2O_2 solutions, and as a carrier. The reagent solution was prepared as follows: 8.0 mg of peroxidase dissolved in 5 ml of phosphate buffer; 0.5 ml of LMG stock

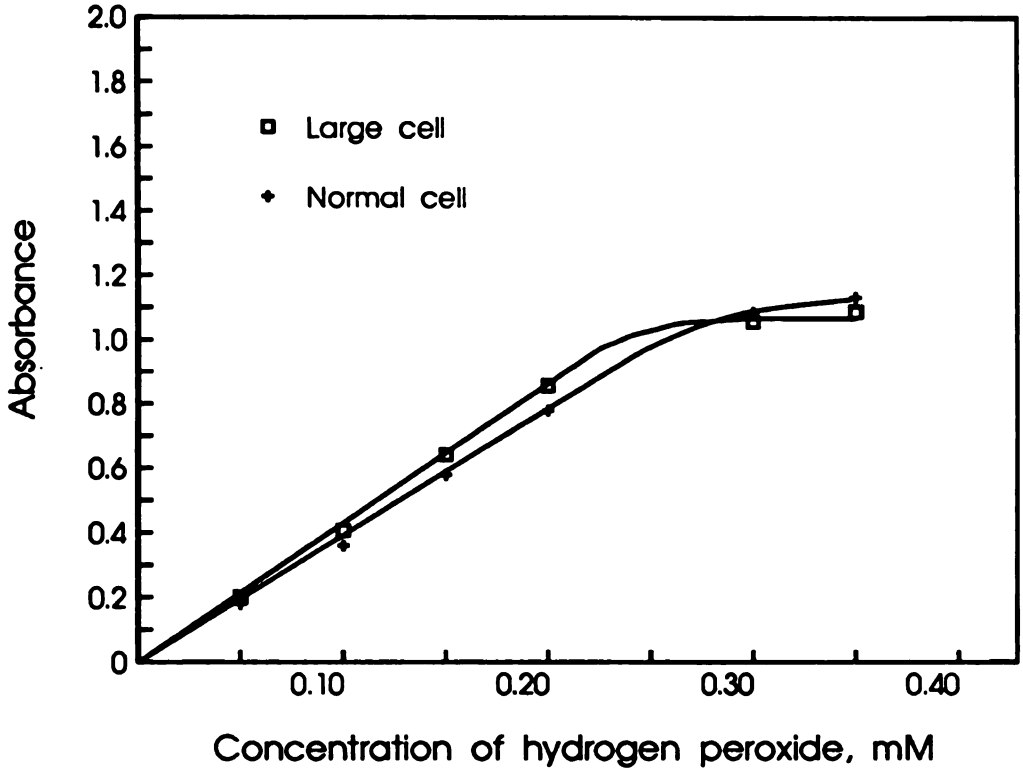

Figure 4-10: Calibration curve using LMG-hydrogen peroxide with stock solution of LMG 1.5 mM using two sizes of observation cells.

solution added and diluted to 10 ml with the same phosphate buffer. The final concentration of LMG in the reagent solution was 0.450 mM. The volume injected was increased to 50 μL. The flow rates were increased to 0.70, 0.53, and 0.08 ml/min for the carrier, the sample, and the reagent respectively (pump setting of 40). The plain SBSR reactor for the detection reaction was increased to 40 cm. The calibration curve was done with the LED detector using the three available LED's (see Figure 3-5) to determine if any important variations in the shape of the calibration curve could be observed by using LED's with different bandwidths of emission.

The results are presented in Figure 4-11. The response was now much higher for both detectors to the extent that only concentrations up to 0.08 mM H_2O_2 could be read with Patton's detector. The slopes for the two detectors were now 4 times higher than in previous experiments (32.9 A/mM for Patton's detector and 14.7 A/mM for the LED detector at 610 nm). This change in slope indicates that the LMG was in fact limiting the reaction, and at lower concentrations of LMG, the reaction was not reaching completion.

As expected, the sensitivity of the curves obtained with the LED's at 640 and 660 nm was much lower. The slopes of the linear parts are 7.3 A/mM for the LED at 640 nm and 6.7 A/mM for the LED at 660 nm.

The curve from Patton's detector shows a negative deviation from linearity starting at 0.08 mM H_2O_2 and completely levels off at 0.10 mM H_2O_2. A similar deviation is observed in the three curves for the LED detector. The strong deviation in Patton's detector may be explained in terms of stray light, since this change was observed at very high values of absorbances. Because the deviations observed in the LED detector

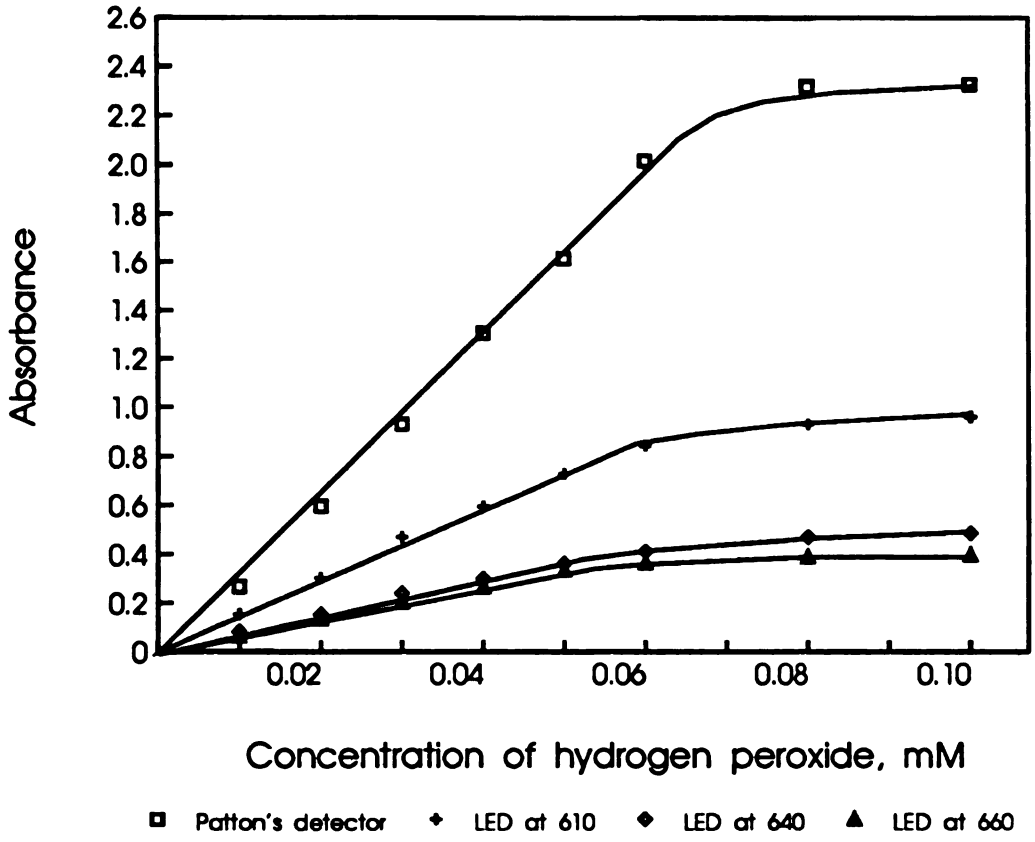

Figure 4-11: Calibration curve using LMG-hydrogen peroxide with stock solution of LMG 9.0 mM. The LED detector was used with the three available LED's.

started at the same concentration as in Patton's detector, it is difficult to conclude that the deviations are due to effects coming from the detector and not from another chemical effect hidden under the deviation from stray light in Patton's detector. This becomes more feasible when one realizes that the effective concentration of LMG in the carrier stream is 0.05 mM due to the different flow rates of carrier and reagent channels, and this is the concentration of H_2O_2 where the deviations occurred.

e. Experiment 5: Effect of non-monochromatic light. In the past four experiments, the response of Patton's detector has been higher than that of the LED detector. This is easily explained by the fact that the filter used in Patton's detector was centered very close to the wavelength of maximum absorbance of malachite green with a bandpass of 20 nm. On the other hand, the LED detector used a source with emission centered on a shoulder of the absorption spectrum of MG and with a broader bandpass. If the bandpass of the LED could be narrowed, the sensitivity of the detector would be increased by increasing the slope of the calibration curve. The linear range should also be increased if the deviation observed so far is due mainly to a non-monochromatic light effect.

One way to reduce the bandpass of the emission from the LED is to use a filter in front of it. In the LED detector this is not so easy to accomplish, but this can be done if the LED is used as the light source in Patton's detector. Two calibration curves were done in this way with and without a filter in Patton's detector. The conditions of the experiment were identical to the ones in Experiment 4, except for the filter used. If a 620 nm filter was used with a 610 nm LED the light throughput was too low to have good detection, so a 610 nm filter was used instead. Still,

the light throughput of the LED-filter combination was much lower (about 10 times) than with the regular tungsten lamp. On the other hand, the LED alone gave a good signal.

The results are shown in Figure 4-12. The calibration curves had slopes of 26.1 A/mM and 18.4 A/mM for the LED-filter combination and the LED alone respectively. This proves that the sensitivity can be increased in the LED detector by decreasing the bandpass of the emission from the LED. On the other hand, the question of the main source of deviation from linearity when a LED is used alone still remains unanswered from the data of this experiment.

There is a small increase in the linear range when a filter is used in front of the LED, meaning that in fact there is some contribution from polychromatic light effects to the deviation observed when using the LED.

Furthermore, the same graph gives evidence that there is another factor causing the deviation. The response of the LED-filter combination is lower than that of tungsten lamp-filter combination. This is explained by the fact that in the first situation, a filter with a center farther from the absorbance maximum of the analyte was used. With the decreased signal, the samples of 0.08 and 0.10 mM H_2O_2 are no longer out of range as they were in the previous experiment, and now they show a similar deviation to the one observed using the LED alone as light source. This could mean that this deviation is actually due to a chemical effect as was suggested previously. On the other hand, there is also the possibility of this deviation being caused in part by stray light. Stray light in Patton's detector comes mainly from ambient light. By using an LED-filter combination the source radiance was decreased tenfold, and

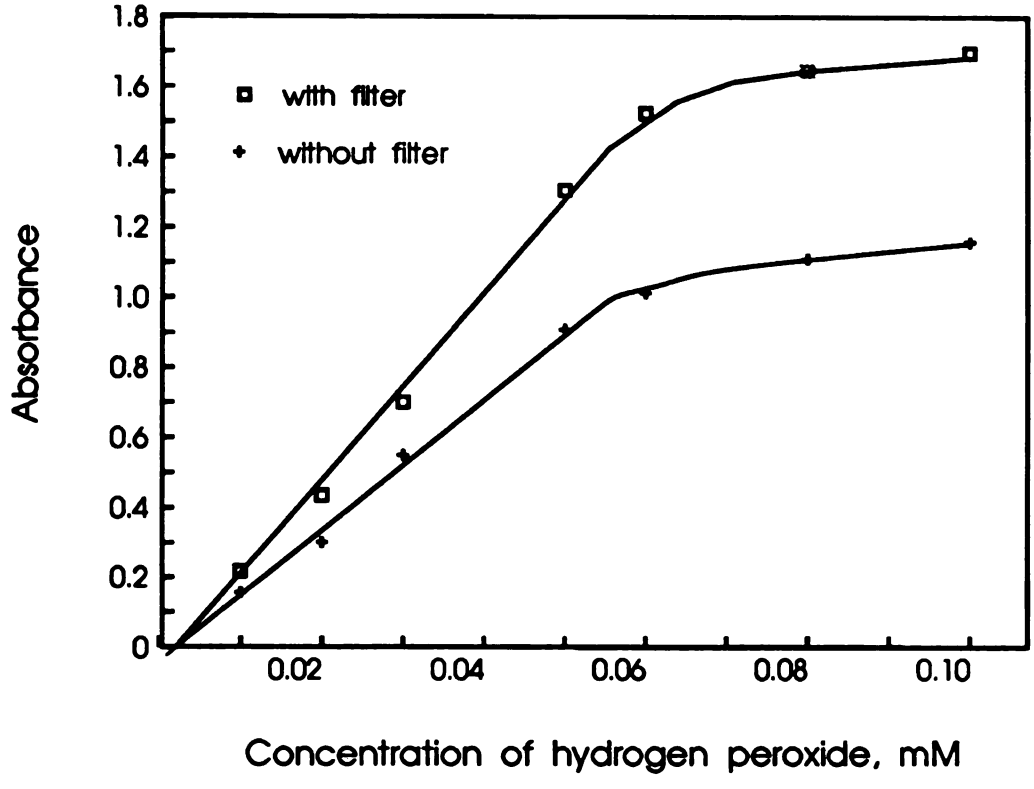

Figure 4-12: Calibration curve using LMG-hydrogen peroxide with stock solution of LMG 10.0 mM. The LED at 610 nm was used in Patton's detector with and without a filter.

this would be the equivalent to increasing the stray light percentage ten times.

Comparing the curves obtained using Patton's detector with the LED and no filter (from Figure 4-12) and the curve using the LED detector (from Figure 4-11), a higher response is still observed with Patton's detector. This could be due to a lower dispersion in the sample zone produced by the cell in Patton's detector as previously discussed.

f. Experiment 6: Effect of the LED forward current. Reducing the forward current of the LED is an easy way to reduce the width of the emission band from the LED. This was tested in an experiment to see if working at low forward currents would improve the performance of the LED detector. Once more, calibration curves using LMG-H_2O_2 were obtained with the LED detector. The conditions were the same as in Experiment 5, and the LED in the detector was first used at 30 mA, the maximum forward current recommended, and then at 10 mA. The results are presented in Figure 4-13.

At the two currents used, there was no noticeable change in the performance of the detector. In fact, the two curves are so similar in the lower points that the experiment could be used to show the repeatability of measurements. The upper points show a variation, but this could be attributed to changes in the reagent solution, which after a period of time starts to degrade.

The possibility of stray light variations at the different forward currents does not agree with the data. In the LED detector the stray light comes mainly from the light passing through the imperfections in the sealant and black paint on the side walls of the observation cell. This means that the stray light should be proportional to the total radiance of

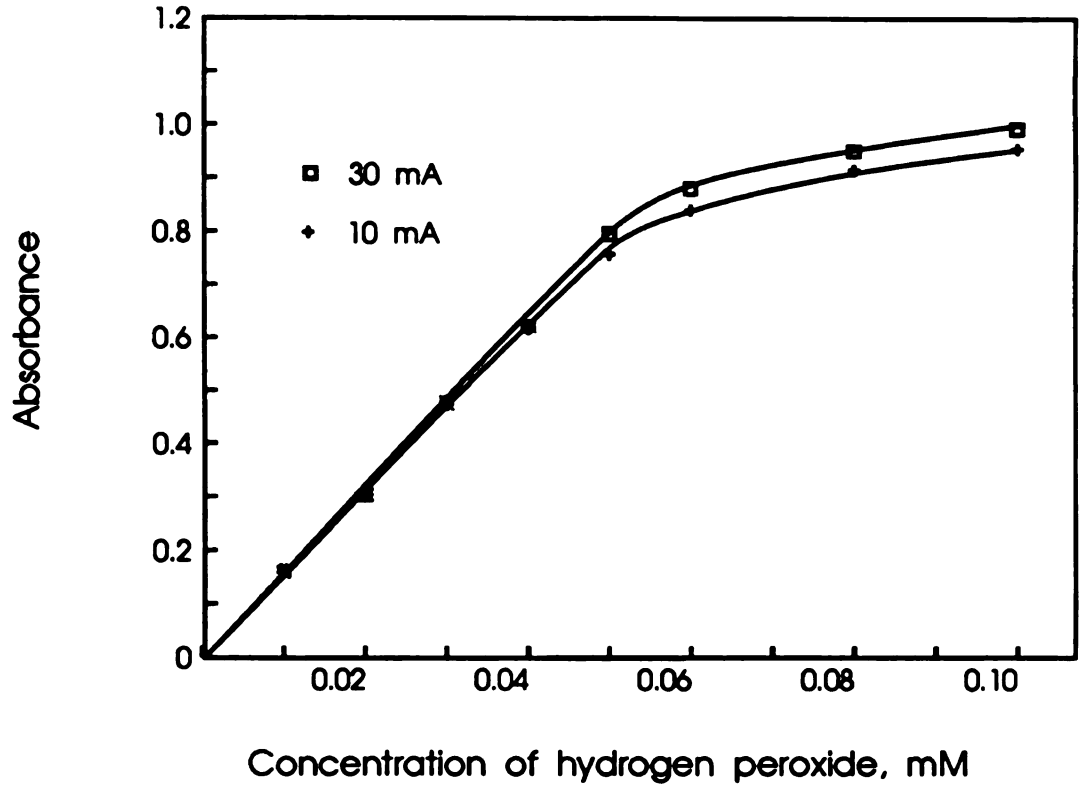

Figure 4-13: Calibration curve using LMG-hydrogen peroxide with stock solution of LMG 10.0 mM. The LED detector was used with LED forward currents of 10 and 30 mA

the LED, so that at higher forward currents a stronger negative deviation should occur. The opposite is observed in Figure 4-13.

The spectra of the LED at two different currents is shown in Figure 4-14. The calculated FWHM is 8 nm larger when the current is increased from 11.6 mA to 20.3 mA. Apparently, the FWHM is already so large that a difference of 8 nm does not have any significant effect on the detector's response.

g. Experiment 7: Calibration curve using a Dye. From the previous experiments, the question of whether a chemical effect or a stray light effect was causing the observed deviation from linearity could not be answered with confidence. Injecting a solution of pure dye reduces the chance of a chemical effect, and, if the dye is chosen correctly, the non-monochromatic light effect can also be reduced. Several pH indicators were tested looking for a relatively flat absorption spectrum in the 610 nm area. The one that meets that condition very well is methylene blue with peaks at 612 nm and 660 nm (Figure 4-15). Unfortunately, methylene blue forms a dimer at high concentrations. The dimer has a higher absorptivity at 600 nm, which produces a positive deviation from Beer's law, and the monomer absorbs stronger at 660 nm producing a negative deviation [42]. Another problem with the dye is that it adheres strongly to glass, and the SBSR's were retaining a lot of the color.

A different manifold was then used which included an open Teflon tube (30 cm) instead of the two SBSR's in the carrier channel. No reagent channel was used. The flow rate was 1 ml/min (pump setting 60). A stock solution 0.2 mM of the dye in pure water was used to prepare injection samples 0.02 mM to 0.2 mM. Calibration curves were

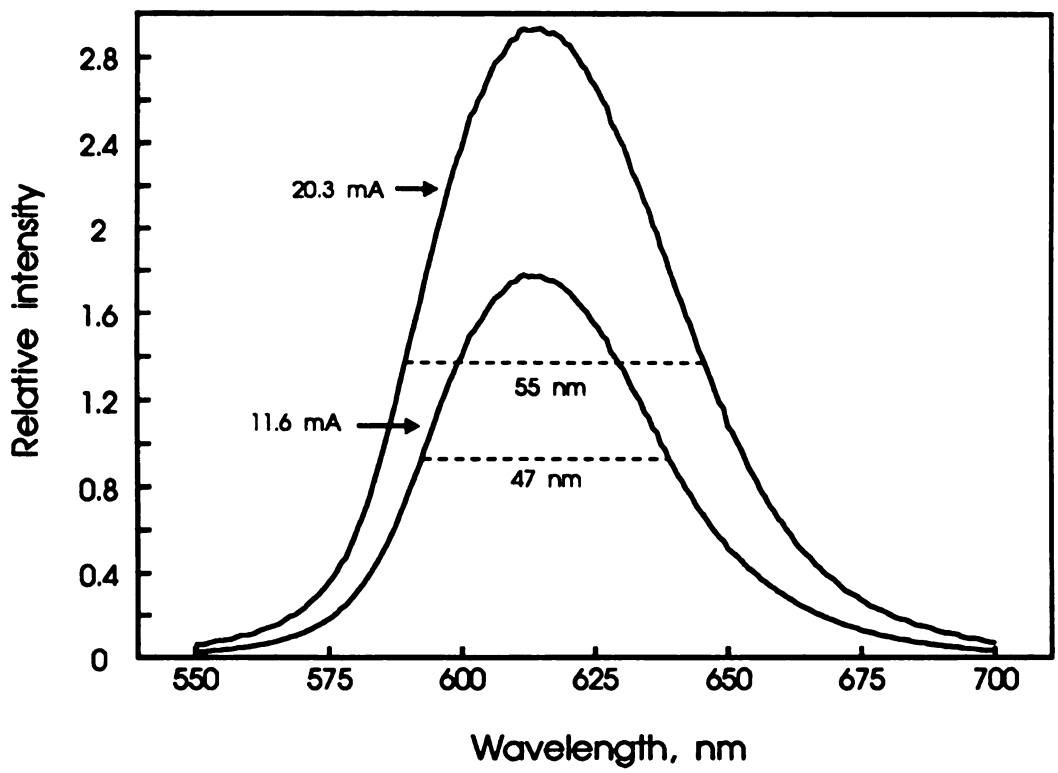

Figure 4-14: Emission spectra for the LED at 610 with low and high forward currents

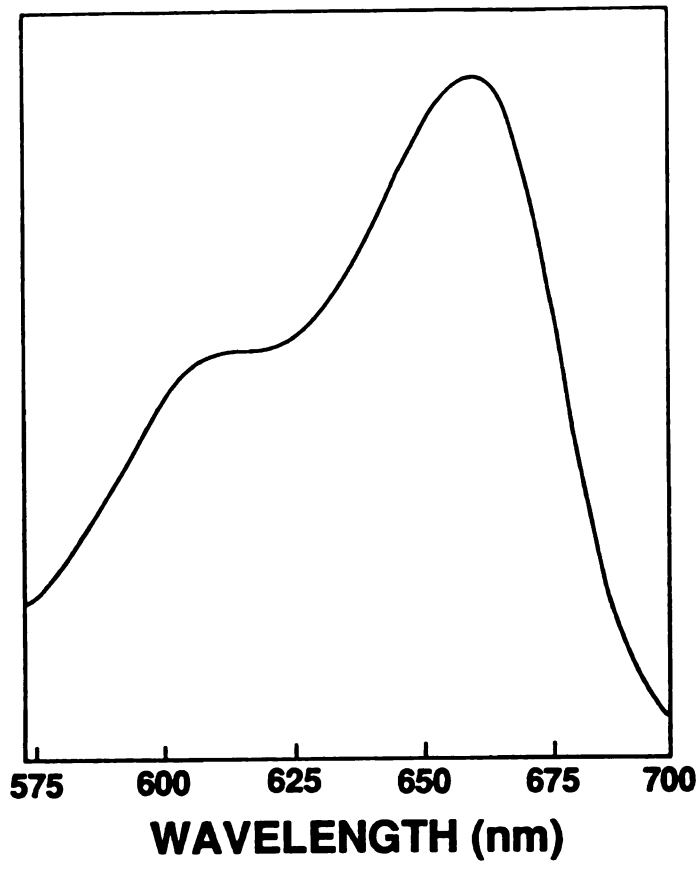

Figure 4-15: Absorption spectrum of methylene blue in water.

prepared at 610 and 660 nm for both detectors. The results are presented in Figure 4-16.

The curve from the LED detector at 610 nm shows a deviation from linearity at absorbances above 1. The curve does not level off as fast as the curves involving LMG-H_2O_2, suggesting that in fact, there was a chemical limitation producing the deviation in those curves. The slope for the linear part of the curve is 10.9 A/nm.

The curve for Patton's detector at 610 nm is linear up to absorbances of 2.4, which confirms the results obtained for the LMG-H_2O_2 reaction. The slope of the regression line is 13.0 A/nm, or 1.2 times higher than the curve with the LED detector. The positive deviation that is observed at 600 nm was not seen at 610 nm, at least for the concentrations studied, perhaps because this wavelength is closer to the isobestic point which is expected at a wavelength between 600 and 660 nm. With methylene blue having a similar absorptivity between 610 and 625 nm, the chances of 610 nm being close to the isobestic point increase. At 660 nm, the negative deviation from linearity starts at low concentrations for both detectors, as expected.

Even with the dimer formation affecting the curve at 660 nm, some interesting conclusions can be drawn from that curve. Comparing the curves at 610 and 660 nm for the LED detector, it is observed that the curve at 610 levels off faster even though the amount of stray light in the detector is expected to be lower at 610 nm because that LED is at least 10 times dimmer. This indicates that the negative deviation at 610 nm might have a stronger effect from non-monochromatic light. Even with the flat area of absorptivity around 615 nm, the bandwidth of emission is so broad for the LED that it seems to be the dominant cause of

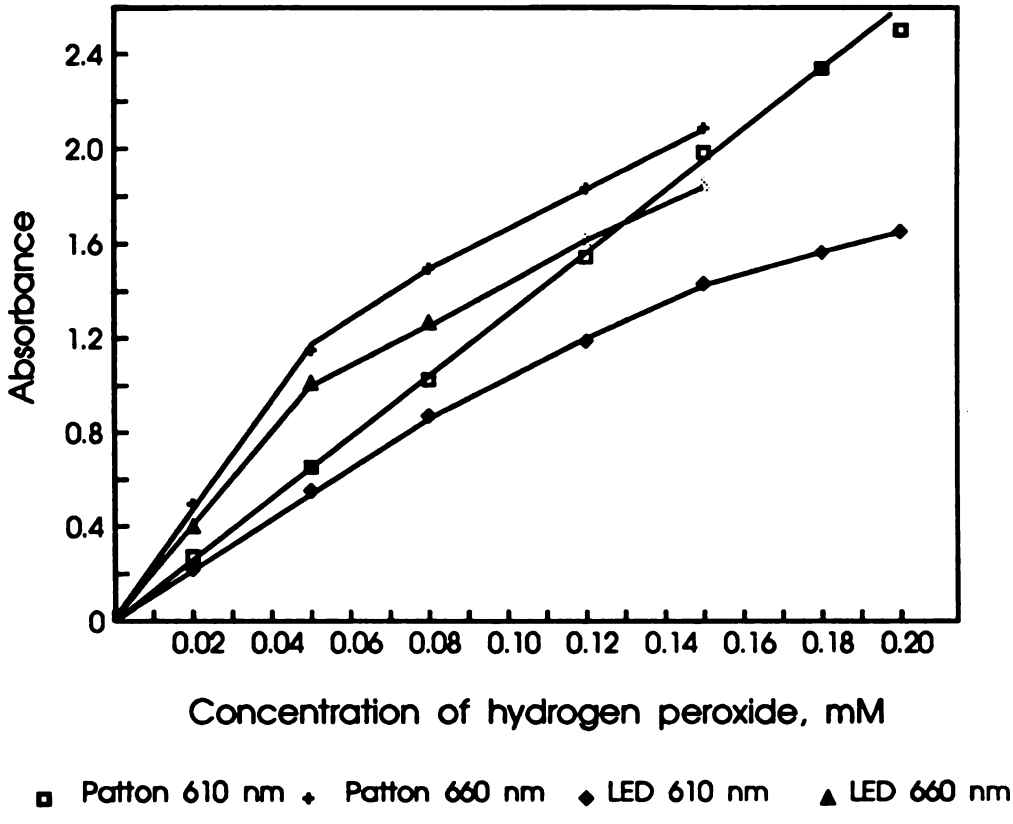

Figure 4-16: Calibration curve using methylene blue with the two detectors at two wavelengths.

non-linearity. In the LMG-H_2O_2 reaction the effect of non-monochromatic light should be stronger and definitely dominant since the measurement is taken on a shoulder of the absorption spectrum.

h. Experiment 8: Calibration curve injecting prepared malachite green. To prove that there was a chemical limitation in the previous LMG-H_2O_2 curves, the reaction was carried out in flasks using a stoichiometric excess of LMG, but still keeping the conditions as close as possible to the ones used in the FIA system. To do this, the proper amount of a stock solution of H_2O_2 (0.256 mM) was added to volumetric flasks to give final H_2O_2 concentrations in the range of 0.01 to 0.15 mM. 50 ml of a reagent solution was prepared by dissolving 40 mg of peroxidase in 20 ml of pH 6.86 phosphate buffer 0.05 M. 5 ml of a 10 mM stock solution of LMG in 37% acetic acid were then added, and the mixture was diluted to 50 ml with phosphate buffer, pH 6.86, giving a final concentration of LMG in the reagent solution of 1 mM. This solution was added to the flasks containing the H_2O_2 in the same proportion to give a dilution of the LMG of 1 to 5. The dark blue-green color appeared immediately and the solutions were then taken to volume with phosphate buffer of pH 6.86. The final solutions were slightly more acidic than the equivalent mixtures in the FIA system due to the increased amount of LMG in acetic acid added. The solutions were then injected in the FIA system using the same manifold and settings of experiment 5.

Figure 4-17 shows a set of peaks obtained with the LED detector for this experiment. Figure 4-18 shows the calibration curves for both detectors. The curve using Patton's detector is again linear to an absorbance of 2, as previously reported. The curve for the LED detector

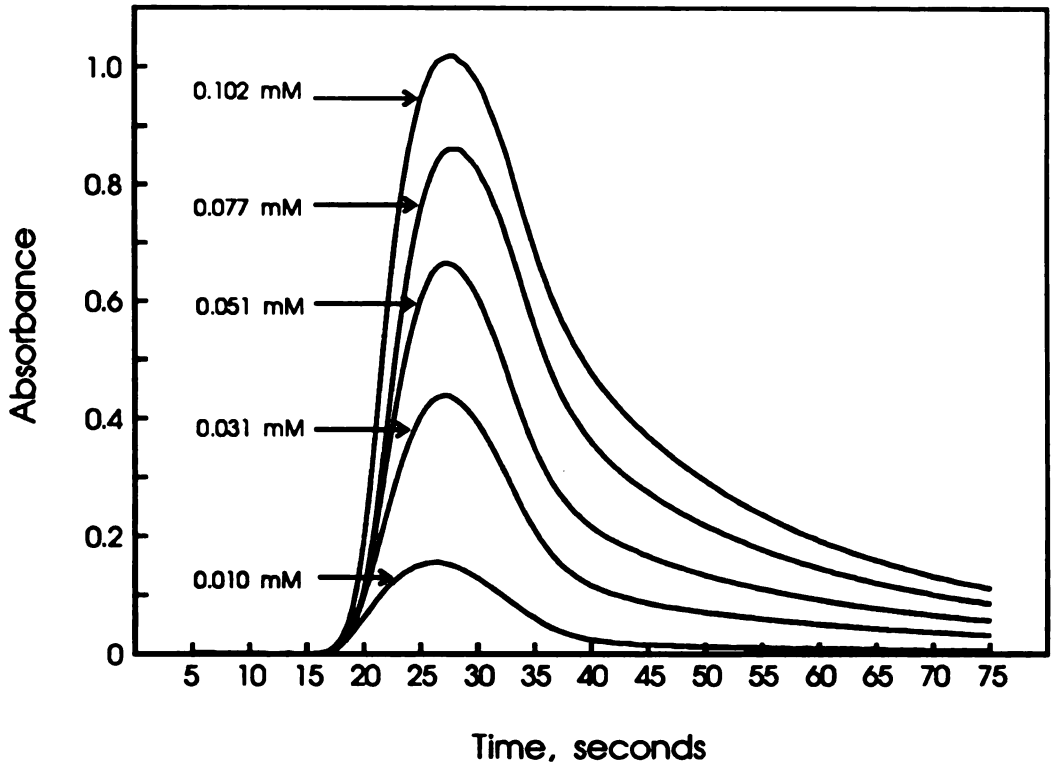

Figure 4-17: FIA peaks observed with the calibration curve using prepared malachite green.

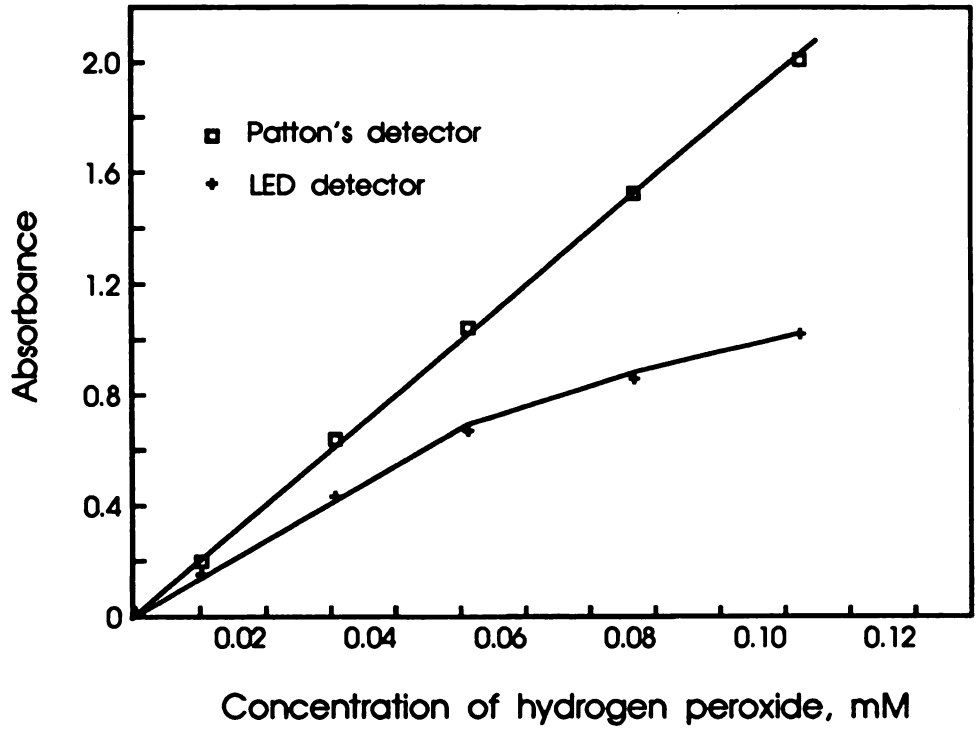

Figure 4-18: Calibration curve using malachite green previously prepared.

shows a smoother deviation from linearity than in previous LMG-H_2O_2 curves indicating that in fact, the chemical system was the limitation in those curves. The deviation observed should be mainly due to the non-monochromatic light effect, and it is comparable to the deviation observed for the methylene blue at 610 nm (Figure 4-16).

The slopes of the regression lines are 19.7 A/nm for Patton's detector and 14.0 A/nm for the LED detector. These slopes keep the same ratio of 1.4 that was observed in previous LMG-H_2O_2 curves.

5. Precision of Measurements:

Any measurement taken by the detector must be taken with an FIA system attached to it, which means that the photometric precision will be affected, and probably limited, by variables from that system. If different measurements taken with any two detectors result in similar repeatability, it could be inferred that the FIA system is limiting the precision, rather than the detectors themselves, or that the two detectors actually have similar repeatability. Two solutions of H_2O_2 were repeatedly injected and measured with the two detectors in question using the conditions described in Experiment 2. A solution of 0.04 mM H_2O_2 was injected 9 times in the FIA system for both detectors (See Figures 4-19 and 4-20). A second solution twice as concentrated was injected 8 times in the FIA system also for both detectors (Figures 4-21 and 4-22). The results are summarized in Table 4-1. Patton's detector shows a lower relative standard deviation (RSD) for both samples. The dependance of the RSD with concentration of H_2O_2 is not clear from these data. An additional source of variation seemed to affect these results: the instability of the reagent solution. It was observed that the last measurements of the set of injections produced lower values than

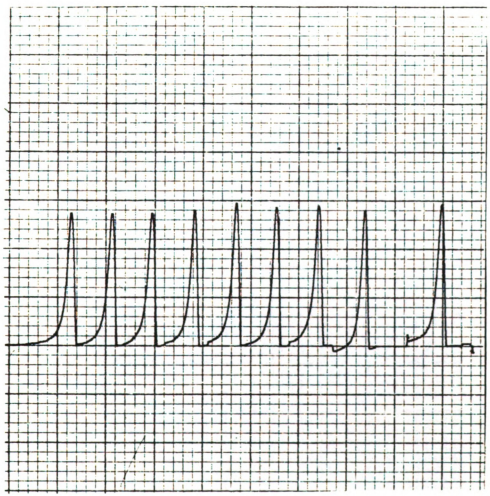

Figure 4-19 **9 injections of a 0.04nM solution of H_2O_2 using the LED-based detector. The RSD of the measured absorance is 2.63%.**

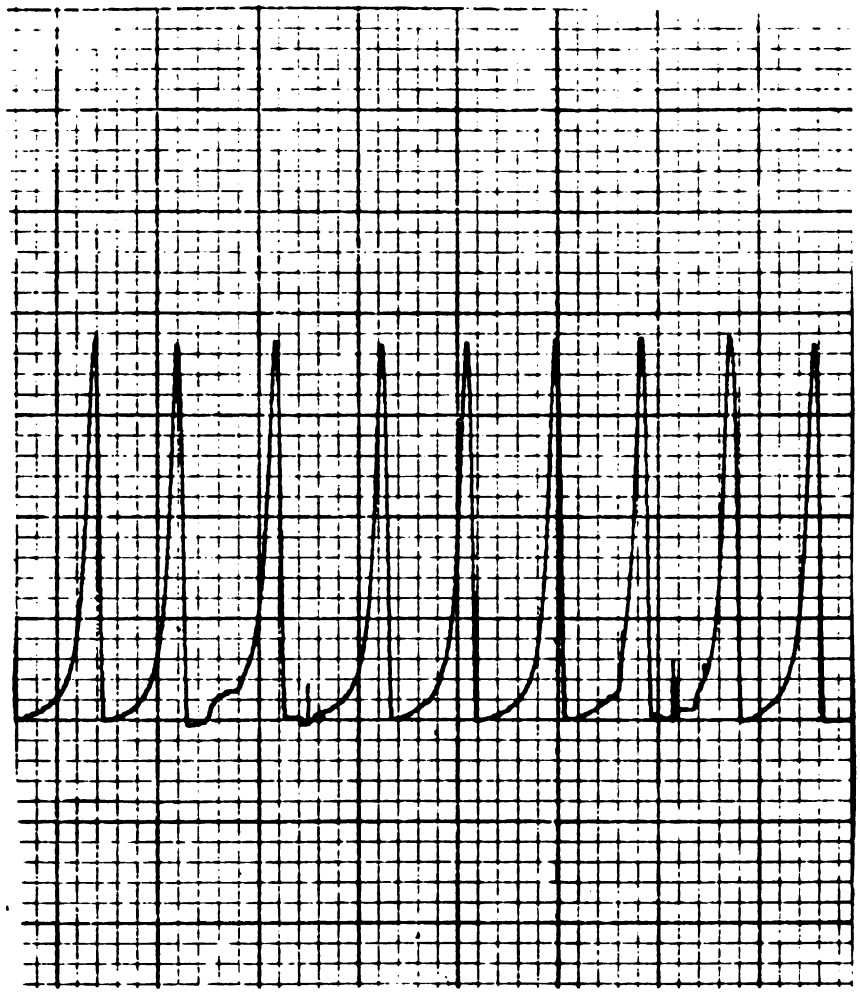

Figure 4-20 **9 injections of a 0.04 mM solution of H202 using Paton's detector. The RSD of the measure absorance is 1.62%**

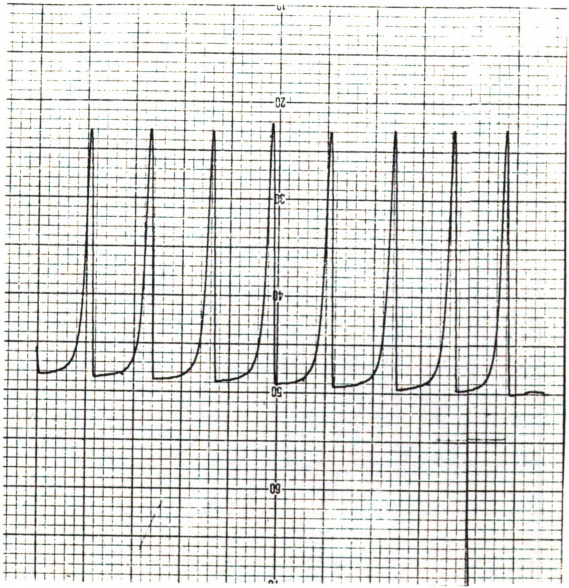

Figure 4-21 **8 injections of a 0.08 MM solution of H2)2 using the LED-based dectector. The RSD of the measured absorbance is 2.25%.**

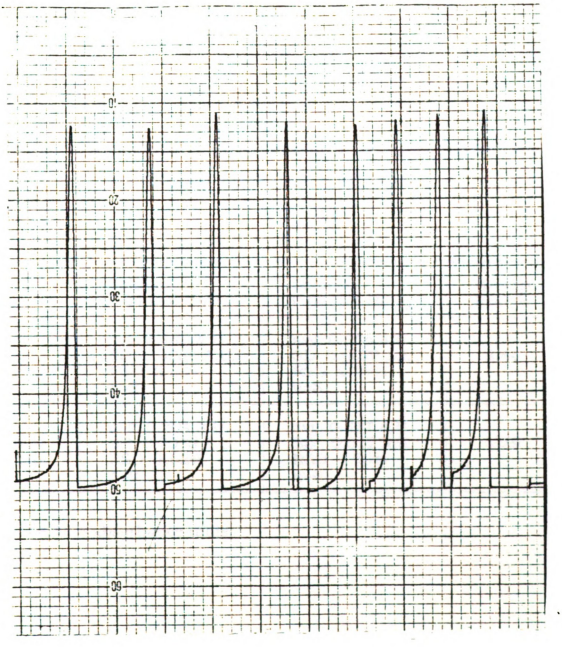

Figure 4-22: 8 injections of a 0.08 mM solution H_2O_2 using Patton's detector. The RSD of the measured absorbance is 1.95%.

Table 4-1:

Results of the experiment of repeatability of measurements with the LED-based and Patton's photometers

	Solution 0.04 mM H_2O_2	Solution 0.08 mM H_2O_2	Average RSD %
LED Detector	avg. 0.143 A.U.* SD 0.0038 A.U. RSD 2.63% n=9	avg. 0.335 A.U. SD 0.0075 A.U. RSD 2.25% n=8	2.44
Current Detector	avg. 0.204 A.U. SD 0.0033 A.U. RSD 1.62% n=9	avg. 0.617 A.U. SD 0.012 A.U. RSD 1.95% n=8	1.79

*A.U. = absorbance units

the initial ones. This may come from some degradation of the reagent solution during the time required to take the measurements.

More information regarding the precision of measurements with both detectors can be obtained from the calibration curves of the experiments in the previous section. Each point in every curve was measured in triplicate so that a RSD can be calculated for each sample. Table 4-2 shows the RSD observed for the points in two calibration curves for both detectors. In both cases the average RSD for the injections with the LED detector was roughly twice that of the injections using Patton's detector. In all the curves, the RSD tends to decrease with higher absorbance readings, an unexpected trend. Normally, if the precision of the absorbance reading is limited by any intrinsic noise from the detector (except for flicker noise), the RSD should increase with higher absorbance values. The observed values then suggest that the precision in the readings may be limited by noise coming from a source external to the detector.

The noise in the output signals of both detectors measured with an oscilloscope is on the order of 4 mV for an output of 1 V when no liquid is flowing through. When there is a flowing liquid present, both detectors show higher noise in the signals due to variations in the flow patterns. As previously discussed, the LED detector is highly sensitive to these variations, and Patton's detector is sensitive as well but to a lower degree. Even when a pulse dampener is used, the pulsations coming from the pump increase the signal noise in both detectors to values higher than 4 mV. This means that in the 100% T baseline reading, the noise is limited by the pump pulsations. However, when a highly absorbing species was present, it was observed that the variation in the

Table 4-2:

Relative Standard Deviations for the triplicate readings of the solutions in two calibration curves

Calibration curve with LMG-H_2O_2

Concentration (mM)	0.01	0.02	0.03	0.04	0.05	0.06	0.10
RSD of measurements with Patton's det.	2.2	1.7	0.3	1.3	0.7	0.1	0.3
RSD of measurements with LED det.	3.0	3.8	0.8	1.9	0.5	2.6	1.9

Calibration curve with Methylene Blue

Concentration (mM)	0.01	0.03	0.05	0.08	0.10
RSD of measurements with Patton's det.	1.3	0.9	1.8	0.5	0.1
RSD of measurements with LED det.	3.7	2.4	2.1	0.9	0.4

output reading decreased for both detectors. This behavior explains the decrease in RSD at high absorbances. A full explanation of the behavior of the flow-through photometers with respect to flow variations is beyond the scope of the present thesis.

In conclusion, the precision of the measurements taken with Patton's detector seems to be twice as high as the precision of measurement with the LED detector, and this is mainly due to a higher sensitivity of the latter to flow variations and not to intrinsic noise within the detector.

6. Detection Limit:

The formula $DL=ks_{bk}/m$ [42] permits the calculation of the detection limit of a determination using a calibration curve, with a confidence level determined by k (k=2 gives a 97.7 confidence level), from the values for s_{bk}, the standard deviation for a blank injection, and m, the slope of the calibration curve. The relative values for these quantities are known for both detectors from the data in the preceding sections so that a relative detection limit can be estimated. In the LED detector, the standard deviation of the blank should be two times that of Patton's detector; and the slope of the calibration curve using the LMG detection reaction should be 0.67 times the slope from Patton's detector. This indicates that the LED detector should have a detection limit three times higher than the detection limit of Patton's detector.

C. PRACTICAL APPLICATION

As a final test for the new LED detector, a real glucose determination was carried out. The procedure suggested by Aspris [6] was followed to determine the glucose content of a sample of commercial

100% apple juice. No special pre-treatment was performed on the sample. 20.0 grams of the juice were diluted to 500 ml using distilled water. 1 ml of this solution was transferred to a 50 ml flask. 1 mg of ascorbate oxidase (1700 u/mg) was dissolved in 0.1 ml phosphate buffer 0.1 M pH 5.5 and the solution was added to the 50 ml flask with the sample to destroy the interfering ascorbic acid. The solution was taken to volume with phosphate buffer 0.05 M pH 6.86. Before injection, the solution was filtered with a No. 1 Whatman filter paper.

Standard glucose solutions 0.04 mM to 0.25 mM were prepared from a 20 mM stock solution using phosphate buffer (0.05 M, pH 6.86) for all the dilutions. 10 ml of the LMG reagent solution were prepared using 8.0 mg of peroxidase and 0.5 ml of 10 mM LMG stock solution and the reagents were diluted with phosphate buffer (0.05 M, pH 6.86). A 10 cm glucose oxidase SBSR was used in the manifold shown in Figure 4-1. 50 µl samples were injected in triplicate. Both detectors were used at a wavelength of 610 nm. The calibration curves are shown in Figure 4-23 and a description of the results follows.

In the case of the LED detector, 4 points were included in the calculation of the regression line giving a slope of 3.79 ± 0.13 A/nm; the average deviation from the regression was 0.021. The reading for the unknown gave a glucose concentration of 0.083 mM with a standard deviation due to the regression of 0.004 mM (4.9% RSD). The last standard point (0.25 mM) was not included in the regression because it showed a definite negative deviation. The average RSD from the triplicate injections was 1.5%. The calculated glucose content for the apple juice was 1.9 ± 0.1 % w/w.

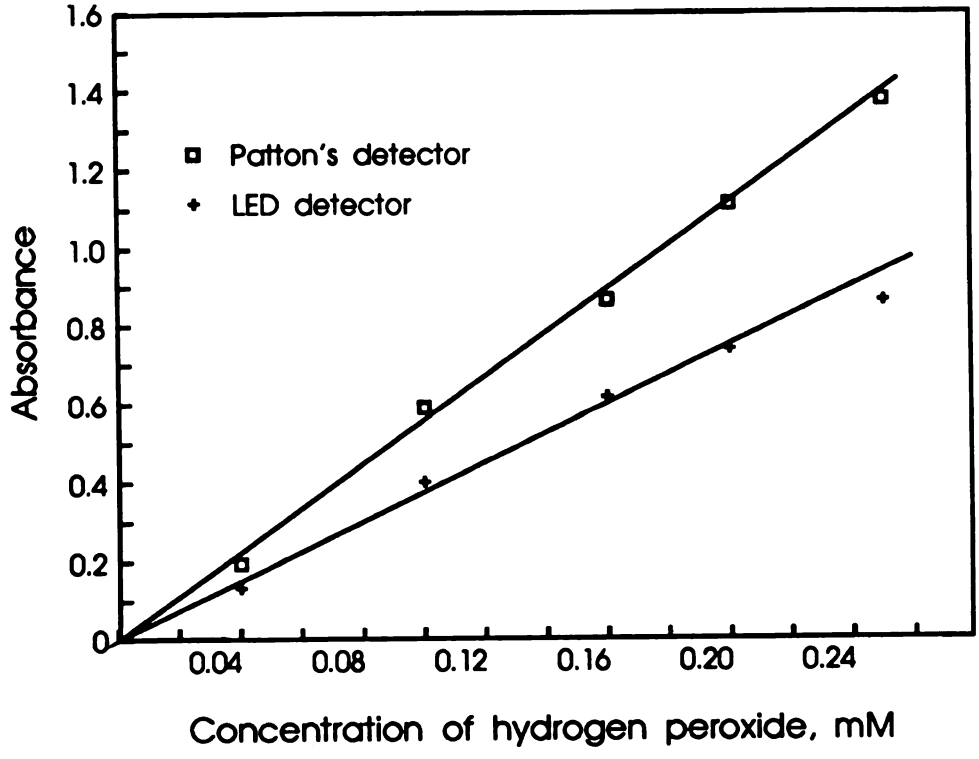

Figure 4-23: Calibration curve for the glucose content determination in apple juice.

In the case of Patton's detector, 5 points were included in the calculation of the regression line giving a slope of 5.55 ± 0.12 A/nm; the average deviation from the regression was 0.025. The reading for the unknown gave a glucose concentration of 0.081 mM with a standard deviation due to the regression of 0.003 mM (4.1% RSD). The average RSD from the triplicate injections was 1.5%. The calculated glucose content for the apple juice was 1.8 ± 0.1 % w/w.

The difference in the two results is not significant with a confidence level of 99%. The sensitivity of the determination as measured from the slopes of the calibration curves was 1.46 times higher in Patton's detector. From the absorbance values observed in the LMG-glucose curve and in the LMG- H_2O_2 one, it can be estimated that a H_2O_2 solution is producing the same absorption as a glucose solution four times as concentrated, meaning that the glucose oxidase reactor is converting 25% of the glucose present. This activity in the reactor is similar to values previously observed [6], even though the enzyme reactor was more than one year old.

CHAPTER V

CONCLUSIONS AND RECOMMENDATIONS

The LED-based photometer constructed offers a simple, low cost option for detection in flow injection analysis, especially for parallel multidetection. The main requirement necessary to be able to use the detector in a given determination is the availability of an LED that emits at a wavelength where the analyte absorbs. In recent times, stronger emitting LED's at many wavelengths in the visible and IR region have become available, making the detector suitable for more applications.

For the sugars analyzer under construction in our laboratories, the detector provides an adequate response within its limitations, when the malachite green reaction is used for the detection. The glucose content of the commercial apple juice determined in the last experiment presented in the previous chapter was in excellent agreement for both the currently used and the LED-based detectors, giving strong evidence of the applicability of the new detector.

The main limitation of the LED detector, when used in a sugar determination with the malachite green reaction, is the low linear range observed. The measurements have to be limited to absorbances below 0.9 if a linear calibration curve is expected. It was concluded from the experiments presented in Chapter IV that the main source of this

deviation was the polychromatic light effect. LED's emit with a relatively broad emission spectrum, and the effect was increased because the measurements were taken on a shoulder of the absorption band of malachite green.

The observed linear range should be suitable for most applications, and an even broader range can be used if a polynomial regression is used. One way of increasing the linear range of the LED detector is to place a filter between the LED and the photodiode. A filter could be used instead of the window in front of the photodiode; also, there are photodiodes available with built-in filters [37]. These options can be implemented if a larger linear range is necessary, and if low operation cost is not so important. It is also expected that new technology will bring improved LED's with narrower emission spectra (the ultrabright LED from Radio Shack is a good example). Laser diodes have very narrow bands of emission; if one emitting in the vicinity of 610 nm is available, it will present another option to improve the linear range of the LED detector.

The other consequence of having a broad bandwidth of emission from the LED is decreased sensitivity. The LED detector always gave calibration curves with slopes 0.7 times the slopes observed with Patton's detector when the malachite green reaction was used.

When compared with the detector currently used, the LED detector showed a lower precision (about half of the other detector) mainly due to a higher sensitivity of the LED detector to the variations in flow in the observed liquid. This lower precision became less important in the enzymatic determination of glucose, because the method itself presented a larger variation, as observed from the calibration curves in Figure 4-23,

and the deviation values from the regression analysis. The determination using the LED detector gave a relative error of 5% against 4% in the determination with the other detector.

A possible way to reduce the sensitivity of the LED detector to the variations in flow, thus increasing its precision, is to use pulsed LED's with synchronous detection.

It was not possible to determine a figure for the percentage of stray light in the LED detector, mainly because the effect of polychromatic light on linearity could not be separated from the stray light effect. The amount of stray light should be low if care is taken in sealing and painting the sides of the observation cell. Special care is needed when the cell is taken apart for cleaning purposes because some of the paint may come off when the lens or the window are removed. If this happens, the cell should be painted again before use.

A summary of some of the figures of merit for the LED detector, as determined from the experiments presented in Chapter IV, is included in Table 5-1.

Table 5-1:

Experimental Results of a Single Photometer

of the Multichannel Detector

Specification	Value	Comments
Wavelength of analysis	610 nm	Other wavelengths available by exchanging LED's.
Spectral bandpass	50 nm	Small variations from LED to LED.
Photometric precision	2.0%	RSD of repeated measurements.
Photometric linear range (A.U.)*	0 to 0.9	with the LMG detection reaction.
Stray light	0.1% or less	a definite value could not be determined.
Baseline noise level (A.U.)	0.002	with a flowing liquid.
Baseline drift (electrical) (A.U./hr.)	0.001	After 15 min. warm-up.
Baseline drift (due to flow) (A.U./min.)	0.001	After 1 hr. of use.

*A.U. = absorbance units

REFERENCES

1. AOAC Official Methods of Analysis, 13th ed. Association of Official Analytical Chemists, Washington D.C., 1980.

2. R. Thompson, Ph.D. Dissertation, Michigan State University, East Lansing, MI, 1982.

3. C. J. Patton, Ph.D. Dissertation, Michigan State University, East Lansing, MI, 1982.

4. C. L. M. Stults, Ph.D. Dissertation, Michigan State University, East Lansing, MI, 1987.

5. K. Kurtz, Ph.D. Dissertation, Michigan State University, East Lansing, MI, 1992.

6. P. Aspris, M.S. Thesis, Michigan State University, East Lansing, MI, 1990.

7. J. Ruzicka and E. H. Hansen, Flow Injection Analysis 2nd Edition, John Wiley and Sons, New York (1988).

8. M. Valcárcel and M. D. Luque de Castro, Flow Injection Analysis: Principles and Applications, John Wiley and Sons, New York (1987).

9. B. Karlberg, *Anal. Chim. Acta* 180, 16 (1986). (In fact, the entire volume 180 of Anal. Chim. Acta is dedicated to FIA).

10. J. Ruzicka, *Fresenius Z. Anal. Chem.* 324, 745 (1986).

11. F. J. Krug, H. Bergamin F°, and E. A. G. Zagatto, *Anal. Chim. Acta* 179, 103 (1986).

12. M. Gallego, M. D. Luque de Castro, and M. Valcárcel, *At. Spectrosc.* 6, 16 (1985).

13. H. Matschiner and P. Sivers, *Wiss. Fortschr.* 35, 142 (1985). [in German].

14. B. Karlberg and G. E. Pacey, Flow Injection Analysis, a Practical Guide, Elsevier, Amsterdam (1989).

15. H. Poppe, *Anal. Chim. Acta* 114, 59 (1980).

16. Y. Baba, N. Yoza, and S. Ohashi, *J. Chromatogr.* 318, 319 (1985).

17. Z. Fang, J. Ruzicka, and E. H. Hansen, *Anal. Chim. Acta* 164, 23 (1984).

18. S. D. Hartenstein, J. Ruzicka, and C. D. Christian, *Anal. Chem.* 57, 21 (1985).

19. G. J. Moody, J. M. Slater, and J. D. R. Thomas, *Anal. Proc.* 23, 287 (1986).

20. J. Ruzicka and E. H. Hansen, *Anal. Chim. Acta* 173, 3 (1985).

21. Visible Light Emitting Diodes, Sharp Technical Data Sheet. Ref. No HT504D, 1987.

22. H. Flaschka, C. McKeitken, and R. Barnes, *Anal. Lett.* 6, 585 (1973).

23. T. Anfält, A. Graneli, and M. Strandberg, *Anal. Chem.* 48, 357 (1973).

24. D. Betteridge, E.L. Dagless, B. Fields, and N.F. Graves, *Analyst* 103, 897 (1978).

25. T.J. Sly, D. Betteridge, D. Wibberley, and D.G. Porter, *J. Autom. Chem.* 4, 186 (1982).

26. D. J. Hooley and R. E. Dessy, *Anal. Chem.* 55, 313 (1983).

27. M. Trojanowicz, W. Augustyniak, and A. Hulanicki, *Mikrochim. Acta* 2, 17 (1984).

28. M. D. Luque de Castro and M. Valcárcel, *Rev. Anal. Chem.* 5, 71 (1986).

29. M. D. Luque de Castro and M. Valcárcel, *Analyst* 109, 413 (1984).

30. M. Valcárcel, M. D. Luque de Castro, F. Lázaro and A. Ríos, *Anal. Chim. Acta* 216, 275 (1989).

31. C. L. M. Stults, A. P. Wade, and S. R. Crouch, *Anal. Chim. Acta* 192, 155 (1987).

32. P. Trinder, *Ann. Clin. Biochem.* 6, 24 (1969).

33. C. J. Patton and S. R. Crouch, *Anal. Chim. Acta* 179, 189 (1986).

34. J. Agranoff (ed.), Modern Plastics Encyclopedia, McGraw-Hill, New York (1983).

35. M. I. Ash, compiler, Encyclopedia of Plastics, Polymers, and Resins Volume II, Chemical Publishing Co., New York (1982).

36. Electro-Optics Handbook, Technical Series EOH-11, RCA Corp., Lancaster, PA., 1974.

37. Photodiodes, Technical Data Sheet, EG&G Photon Devices, Salem MA.

38. C. E. Evans, J. G. Shabushnig, and V. L. McGuffin, *J. Chromatogr.* 459, 119 (1988).

39. J. Lown, R. Koile, and D. Johnson, *Anal. Chim. Acta* 116, 33 (1980).

40. H. Bergamin, B. Reis, and E. Zagatto, *Anal. Chim. Acta* 97, 427 (1978).

41. H. Poppe, *Anal. Chim. Acta* 145, 17 (1983).

42. J.D. Ingle and S.R. Crouch, Spectrochemical Analysis, Prentice Hall, New Jersey (1988).

MICHIGAN STATE UNIV. LIBRARIES
31293007927365